



HAL
open science

Hindbrain catecholaminergic inputs to the paraventricular thalamus scale feeding and metabolic efficiency in stress-related contexts

Clarisse Dumont, Guangping Li, Julien Castel, Serge Luquet, Giuseppe Gangarossa

► To cite this version:

Clarisse Dumont, Guangping Li, Julien Castel, Serge Luquet, Giuseppe Gangarossa. Hindbrain catecholaminergic inputs to the paraventricular thalamus scale feeding and metabolic efficiency in stress-related contexts. 2022. hal-03846811

HAL Id: hal-03846811

<https://hal.science/hal-03846811>

Preprint submitted on 10 Nov 2022

HAL is a multi-disciplinary open access archive for the deposit and dissemination of scientific research documents, whether they are published or not. The documents may come from teaching and research institutions in France or abroad, or from public or private research centers.

L'archive ouverte pluridisciplinaire **HAL**, est destinée au dépôt et à la diffusion de documents scientifiques de niveau recherche, publiés ou non, émanant des établissements d'enseignement et de recherche français ou étrangers, des laboratoires publics ou privés.

27 **Key points**

28

29 1. The paraventricular thalamus (PVT) is known to receive projections from the
30 hindbrain. Here, we confirm and further extend current knowledge on the existence of
31 hindbrainTH→PVT catecholaminergic (CA) inputs, notably from the locus coeruleus
32 (LC) and the nucleus tractus solitarius (NTS), with the NTS representing the main
33 source.

34

35 2. Disruption of hindbrainTH→PVT inputs contribute to the modulation of PVT-
36 neurons activity.

37

38 3. HindbrainTH→PVT inputs scale feeding strategies in environmental, behavioral,
39 physiological and metabolic stress-like contexts.

40

41 4. HindbrainTH→PVT inputs participate in regulating metabolic efficiency and nutrient
42 partitioning in stress-like contexts.

43

44 5. HindbrainTH→PVT, directly and/or indirectly, contribute in modulating the
45 downstream activity of lateral (LH) and dorsomedial (DMH) hypothalamic neurons.

46 **Abstract**

47

48 The regulation of food intake and energy balance relies on the dynamic integration of
49 exteroceptive and interoceptive signals monitoring nutritional, metabolic, cognitive
50 and emotional states. The paraventricular thalamus (PVT) is a central hub that, by
51 integrating sensory, metabolic and emotional states, may contribute to the regulation
52 of feeding and homeostatic/allostatic processes. However, the underlying PVT
53 circuits remain still elusive. Here, we aimed at unraveling the role of
54 catecholaminergic (CA) inputs to the PVT in scaling feeding and metabolic efficiency.
55 First, using region-specific retrograde disruption of CA projections, we show that PVT
56 CA inputs mainly arise from the hindbrain, notably the locus coeruleus (LC) and the
57 nucleus tractus solitarius (NTS). Second, taking advantage of integrative calorimetric
58 measurements of metabolic efficiency, we reveal that CA inputs to the PVT scale
59 adaptive feeding and metabolic responses in environmental, behavioral,
60 physiological and metabolic stress-like contexts. Third, we show that
61 hindbrainTH→PVT inputs contribute in modulating the activity of PVT as well as
62 lateral (LH) and dorsomedial (DMH) hypothalamic neurons.

63 In conclusion, this study, by assessing the key role of CA inputs to the PVT in scaling
64 homeostatic/allostatic regulations of feeding patterns, reveals the integrative and
65 converging hindbrainTH→PVT paths that contribute to whole-body metabolic
66 adaptations in stress-like contexts.

67 Introduction

68

69 In mammals, the regulation of food intake intricately relies on the orchestration of
70 several signals mirroring the dynamic integration of interoceptive and exteroceptive
71 (environment) states (Sweeney & Yang, 2017). Indeed, emotional states (stress,
72 anxiety, motivation), by modulating the activity of central neuronal hubs, thoroughly
73 scale the regulation of food intake and the establishment of feeding habits (Ulrich-Lai
74 *et al.*, 2015). This is particularly evident in stress-related contexts where emotional
75 states compete with the homeostatic regulation of feeding (Maniam & Morris, 2012;
76 Herzog, 2020), thereby leading to feed-forward allostatic adaptations (*stability*
77 *through changes*) which may culminate in psychiatric and metabolic disorders. These
78 observations support the idea that emotional and homeostatic states may share
79 similar, although not identical, neuronal networks (Sweeney & Yang, 2017).
80 Nonetheless, the systems underlying the functional connection between these states
81 remain poorly understood.

82 Emerging evidence strongly suggests that the paraventricular nucleus of the
83 thalamus (PVT), a dorsal midline thalamic relay, may represent a functional *hot-spot*
84 where interoceptive and exteroceptive stimuli may converge to orchestrate the
85 selection of adaptive and appropriate behavioral responses aimed at regulating
86 homeostatic and cognitive processes (Penzo & Gao, 2021). Given their elaborated
87 connectivity (Kirouac, 2015), PVT excitatory (glutamate) neurons are well positioned
88 to serve as functional integrators of orexigenic and anorexigenic stimuli (Ong *et al.*,
89 2017; Meffre *et al.*, 2019), glucose fluctuations (Labouèbe *et al.*, 2016; Kessler *et al.*,
90 2021), learning and memory processes (Do-Monte *et al.*, 2015; Penzo *et al.*, 2015)
91 as well as emotional states (Heydendael *et al.*, 2011; Barson *et al.*, 2020; Pliota *et*
92 *al.*, 2020). This plethora of PVT-related brain functions highly relies on different
93 afferent projections which, by carrying distinct neurochemical information,
94 synergistically scale the activity of PVT-neurons and their downstream connected
95 regions. Among the different afferents, the PVT also harbors a dense plexus of
96 catecholaminergic (CA) fibers mainly arising from the hindbrain (Schroeter *et al.*,
97 2000; Beas *et al.*, 2018; Sofia Beas *et al.*, 2020; Wang *et al.*, 2021*b*) and only few
98 scattered CA fibers from the hypothalamus (Li *et al.*, 2014). In addition, recent
99 reports have indicated that brain CA (norepinephrine, NE, and/or dopamine, DA), by
100 modulating different homeostatic functions (*i.e.* wakefulness, arousal, glucoprivation-

101 induced food seeking), may represent key neuromodulators of the PVT (Beas *et al.*,
102 2018; Sofia Beas *et al.*, 2020; Wang *et al.*, 2021b). Moreover, brain CA are also
103 important contributors to the regulation of stress-like responses (Valentino & Van
104 Bockstaele, 2008; Kvetnansky *et al.*, 2009) which ultimately impact, directly and/or
105 indirectly, on feeding patterns and behaviors (Xu *et al.*, 2019; Qu *et al.*, 2020).
106 Indeed, the PVT has already been involved in food-seeking behaviors mostly
107 associated to positive (motivation, reward, reinforcement) or negative valance
108 (Labouèbe *et al.*, 2016; Otis *et al.*, 2017, 2019; Do-Monte *et al.*, 2017; Wang *et al.*,
109 2021a; Engelke *et al.*, 2021) as well as in stress and emotional arousal (Hsu *et al.*,
110 2014). However, whether and how the PVT and its afferent CA inputs may contribute
111 to the regulation of food intake and metabolic efficiency in stress-related contexts
112 remain to be fully established.

113 In order to dissect the contribution of PVT CA inputs in the regulation of food intake,
114 we suppressed local CA inputs by microinjecting the neurotoxin 6-OHDA into the
115 PVT and performed several experiments aimed at revealing the adaptive strategies
116 associated to the regulation of feeding and energy balance. Here, we demonstrate
117 that CA inputs to the PVT exerted a modulatory role on food intake and metabolic
118 efficiency specifically in stress-related contexts since no major alterations were
119 detected in basal conditions. Notably, we found that 6-OHDA^{PVT}-lesioned mice,
120 following both exteroceptive (environmental) and interoceptive (body energy)
121 stressors, showed enhanced food intake and metabolic efficiency.

122 Altogether, our results reveal a novel neuronal network by which stressors impinge
123 on the regulatory allostatic processes underlying feeding behaviors, metabolic
124 efficiency and nutrient partitioning to scale stress-associated adaptive responses.

125 **Materials and methods**

126

127 **Ethics statement and animals**

128 All experiments were approved by the Animal Care Committee of the Université Paris
129 Cité (APAFiS #35585 and #11003) and carried out following the 2010/63/EU
130 directive. 8-14 weeks old male C57Bl/6J mice (Janvier, Le Genest St Isle, France)
131 were used and housed in a room maintained at 22 +/-1 °C, with a light period from
132 7h00 to 19h00. Regular chow diet (3.24 kcal/g, reference SAFE® A04, Augy, France)
133 and water were provided *ad libitum* unless otherwise stated.

134

135 **Stereotaxic microinjections for viral tracing studies and 6-OHDA-induced**
136 **catecholaminergic denervation**

137 Mice were anaesthetized with isoflurane (3.5% for induction, 1.5% for maintenance),
138 administered with Buprécare® (buprenorphine 0.3 mg) and Ketofen® (ketoprofen 100
139 mg), and placed on a stereotactic frame (Model 940, David Kopf Instruments). During
140 surgery, body temperature was maintained at 37°C.

141 6-OHDA-HCl (Sigma-Aldrich, #H4381) was dissolved in a saline solution (NaCl 0.9%
142 w/v) containing 0.02% of ascorbic acid at a final concentration of 6 µg/µl. Animals
143 were randomly assigned to either 6-OHDA or vehicle microinjections. A volume of
144 0.35 µl of 6-OHDA or vehicle (0.02% ascorbic acid) was injected into the PVT (L=
145 0.0; AP= -1.46; V= -2.8, mm) at an infusion rate of 0.05 µl/min. The injection needle
146 was carefully removed after waiting 5 minutes at the injection site. 24-hrs after,
147 animals were re-administered with Buprécare® and Ketofen®, and had facilitated
148 access to jelly food (DietGel Boost #72-04-5022, Clear H₂O) for 2 consecutive days.
149 Recovery from surgery was monitored during 3-5 days post-surgery. Animals were
150 allowed to recover for 3-4 weeks before any experimental evaluation.

151 pAAV-CAG-tdTomato (titer $\geq 1 \times 10^{13}$ vg/mL) was a gift from Edward Boyden
152 (Addgene viral prep #59462-AAV9; <http://n2t.net/addgene:59462>;
153 RRID:Addgene_59462). A volume of 0.20 µl of pAAV-CAG-tdTomato was injected
154 into the PVT (L= 0.0; AP= -1.46; V= -2.8, mm) at an infusion rate of 0.05 µl/min. The
155 injection needle was carefully removed after waiting 5 minutes at the injection site.
156 Viral expression was evaluated 4 weeks after microinjection.

157

158 **Indirect calorimetry and metabolic efficiency analysis**

159 Indirect calorimetry was performed as previously described (Berland *et al.*, 2022).
160 Mice were monitored for whole energy expenditure (EE), O₂ consumption and CO₂
161 production, respiratory exchange rate (RER=VCO₂/VO₂), fatty acid oxidation (FAO),
162 and locomotor activity using calorimetric cages with bedding, food and water
163 (Labmaster, TSE Systems GmbH, Bad Homburg, Germany). Ratio of gases was
164 determined through an indirect open circuit calorimeter (Arch *et al.*, 2006; Even &
165 Nadkarni, 2012). This system monitors O₂ and CO₂ concentration by volume at the
166 inlet ports of a tide cage through which a known flow of air is being ventilated (0.4
167 L/min) and compared regularly to a reference empty cage. For optimal analysis, the
168 flow rate was adjusted according to the animal body weights to set the differential in
169 the composition of the expired gases between 0.4-0.9% (Labmaster, TSE Systems
170 GmbH, Bad Homburg, Germany). The flow was previously calibrated with O₂ and
171 CO₂ mixture of known concentrations (Air Liquide, S.A. France). O₂ consumption and
172 CO₂ production were recorded every 15 min for each animal during the entire
173 experiment. Whole energy expenditure (EE) was calculated using the Weir equation
174 for respiratory gas exchange measurements. Food consumption was measured as
175 the instrument combines a set of highly sensitive feeding sensors for automated
176 online measurements. Mice had access to food and water *ad libitum*. To allow
177 measurement of every ambulatory movement, each cage was embedded in a frame
178 with an infrared light beam-based activity monitoring system with online
179 measurement at 100 Hz. The sensors for gases and detection of movements
180 operated efficiently in both light and dark phases, allowing continuous recording.
181 When required, the inversion of circadian light/dark cycles was programmed using
182 the Labmaster software.

183 Body mass composition was analyzed using an Echo Medical systems' EchoMRI
184 (Whole Body Composition Analyzers, EchoMRI, Houston, USA), according to
185 manufacturer's instructions. Readings of body composition were given within 1 min.
186 Data analysis was performed on Excel XP using extracted raw values of VO₂
187 consumed (expressed in ml/h), VCO₂ production (expressed in ml/h), and energy
188 expenditure (kcal/h).

189

190 **Novelty-suppressed feeding (NSF)**

191 After an overnight fasting, mice were placed in a cage (40×40×40 cm) with a single
192 regular chow pellet in the center. The latency (time in seconds) to eat was scored. To
193 measure food intake, food consumption was evaluated 60 minutes after the
194 beginning of the test.

195

196 **Open field (OF)**

197 Spontaneous exploratory behavior was monitored in an open field (40×40×40 cm,
198 BIOSEB) for 20 min, video-tracked and analyzed using the SMART software
199 (BIOSEB). The open field was wiped with 70% ethanol between sessions.

200

201 **Infrared temperature measurements**

202 Thermogenesis was visualized using a high-resolution infrared camera (FLIR E8;
203 FLIR Systems, Portland, OR, USA). To measure the temperature (°C) of the brown
204 adipose tissue (BAT, interscapular regions), lower back and tail, images were
205 captured before and after the open field (OF) test. Infrared thermography images
206 were analyzed using the FLIR TOOLS software.

207

208 **Food intake following food or water deprivation**

209 In two distinct experiments we measured food intake following either an overnight
210 fasting (food deprivation) or water deprivation.

211 *Overnight fasting.* Mice were first weighted in the morning following an overnight
212 fasting to ensure the loss of body weight. Then, they were exposed to pre-weighted
213 chow pellets. Food intake was measured at the following time points: 30 min, 1h, 2h,
214 3h, 4h.

215 *Overnight water deprivation.* Mice were first weighted in the morning following an
216 overnight water deprivation to ensure the loss of body weight. Then, they were
217 exposed to a calibrated drinking bottle and pre-weighted chow pellets. Water
218 consumption and food intake were measured at the following time points: 30 min, 1h,
219 2h, 3h, 4h.

220

221 **Food intake induced by 2-DG and ghrelin**

222 Mice were handled and injected with vehicle during 3 consecutive days before drugs
223 administration. After this habituation period, they were administered with ghrelin
224 (#1465, Tocris, 0.5 mg/kg, i.p.) or 2-DG (#14325, Cayman Chemical, 500 mg/kg, i.p.)

225 and exposed to chow pellets 30 min after the injections. Food intake was measured
226 during 3 hours. For 2-DG treated mice, blood glucose (counterregulatory response)
227 was measured from the vein tail using a glucometer (Menarini Diagnostics, Rungis,
228 France) at 0 and 30 min.

229

230 **Glucose dynamics**

231 *Oral glucose tolerance test (OGTT)*. Animals were fasted 5 hours before receiving a
232 bolus of glucose solution (2 g/kg) by gavage. Blood glucose (hyperglycemia) was
233 measured from the vein tail using a glucometer (Menarini Diagnostics, Rungis,
234 France) at 0, 5, 10, 15, 30, 60, 90, and 120 min.

235 *Insulin tolerance test (ITT)*. Animals were fasted 5 hours before receiving an injection
236 of insulin (0.5 U/kg, Novo Nordisk, i.p.). Blood glucose (hypoglycemia) was measured
237 from the vein tail at 0, 5, 10, 15, 20, 30, 60, 90, and 120 min.

238

239 **Tissue preparation and immunofluorescence**

240 Animals were injected with pentobarbital (500 mg/kg, i.p., Sanofi-Aventis, France).
241 Once anaesthetized, they were transcardially perfused with cold (4°C) PFA 4% for 5
242 minutes. Brains were collected, put overnight in PFA 4% and then stored in PBS
243 (4°C). 40 µm-thick sections were sliced with a vibratome (Leica VT1000S, France)
244 and stored in a cryoprotective solution at -20 °C until immunofluorescence
245 investigations. Immunofluorescence on brain slices was performed as previously
246 described (Gangarossa *et al.*, 2019; Berland *et al.*, 2020).

247 Briefly, sections were processed as it follows. Day 1: free-floating sections were
248 rinsed in Tris-buffered saline (TBS; 0.25 M Tris and 0.5 M NaCl, pH 7.5), incubated
249 for 5 min in TBS containing 3% H₂O₂ and 10% methanol, and then rinsed three times
250 for 10 min each in TBS. After 15 min incubation in 0.2% Triton X-100 in TBS,
251 sections were rinsed three times in TBS again. Slices were then incubated 48 hrs at
252 4°C with the following primary antibodies: rabbit anti-cFos (1:1000, Synaptic
253 Systems, #226 003), rabbit anti-TH (1:1000, Millipore, #AB153) or rat anti-DAT
254 (1:500, Millipore, #MAB369). Sections were rinsed three times for 10 min in TBS and
255 incubated for 60 min with secondary donkey anti-rabbit Cy3 AffiniPure (1:1000,
256 Jackson ImmunoResearch, #711-165-152) or donkey anti-rat Cy3 AffiniPure (1:1000,
257 Jackson ImmunoResearch, #712-165-153). Sections were rinsed for 10 min twice in
258 TBS, stained with DAPI (10 min) and rinsed in TB (0.25 M Tris) before mounting.

259 Acquisitions were performed with a confocal microscope (Zeiss LSM 510). The
260 objective (10X) and the pinhole setting remained unchanged during the acquisition of
261 a series for all images. Depending on the extension of the region of interest, either
262 single or mosaic acquisitions were conducted. Quantification of immunoreactive cells
263 (cFos- or TH-positive neurons) was performed using the cell counter plugin of the
264 ImageJ software taking as standard reference a fixed threshold of fluorescence. For
265 cell counting, three (TH) or two (cFos) rostro-caudal levels for each brain region were
266 used. Quantifications of immunopositive neurons were averaged between
267 hemispheres and then summed for consecutive brain slices.

268

269 **Statistics**

270 All data are presented as mean \pm SD. Statistical tests were performed with Prism 7
271 (GraphPad Software, La Jolla, CA, USA). Detailed statistical analyses are listed in
272 the **Statistical Summary Table**. Normality was assessed by the D'Agostino-Pearson
273 test. Depending on the experimental design, data were analyzed using either Student
274 t-test (paired or unpaired) with equal variances, One-way ANOVA or Two-way
275 ANOVA. The significance threshold was automatically set at $p < 0.05$. ANOVA
276 analyses were followed by Bonferroni *post hoc* test for specific comparisons only
277 when overall ANOVA revealed a significant difference (at least $p < 0.05$).

278 **Results**

279

280 **Catecholaminergic inputs modulate the activity of PVT-neurons**

281 To study whether catecholaminergic (TH-positive) inputs to the PVT
282 participate/contribute to the regulation of food intake, we decided to ablate
283 catecholamine (CA) fibers projecting to the PVT by locally microinjecting 6-OHDA
284 (**Figure 1A**), a neurotoxin reuptaken by DAT- and/or NET-expressing terminals.
285 Since the PVT extends throughout the midline thalamic axis, we decided to mainly
286 focus on the mid-posterior PVT as this region has been shown to be involved in
287 stress and stress-induced hypophagia (Heydendael *et al.*, 2011; Barson *et al.*, 2020;
288 Barrett *et al.*, 2021). Indeed, 6-OHDA was able to strongly reduce TH
289 immunostaining in the PVT (**Figure 1B**), with few remaining terminals most likely
290 corresponding to NET-negative TH fibers (terminals releasing adrenaline and/or
291 devoid of monoamine transporters) since the PVT does not seem to contain DAT-
292 positive terminals as compared to DAT-rich regions such as the tail of the striatum
293 [TS, (Gangarossa *et al.*, 2013; Valjent & Gangarossa, 2021)] and the central
294 amygdala (**Suppl. Figure 1A**, <https://doi.org/10.6084/m9.figshare.19683228.v1>).

295 We therefore examined the regional sources of our 6-OHDA-induced degeneration of
296 TH-afferents. We focused on putative noradrenergic TH-positive projecting neurons
297 since the PVT do not receive dopaminergic inputs from the midbrain (SNc and VTA)
298 (Li *et al.*, 2014) and it harbors only minor, if any, scattered DAT-fibers (García-
299 Cabezas *et al.*, 2009; Clark *et al.*, 2017). Immunofluorescence analysis revealed a
300 significant reduction of TH-neurons in the nucleus tractus solitarius (NTS) and the
301 locus coeruleus (LC), in line with the presence of *Slc6a2* (NET)-catecholaminergic
302 neurons in these nuclei (Schroeter *et al.*, 2000; Zhang *et al.*, 2021) and the sensitivity
303 of these neurons to 6-OHDA (Szot *et al.*, 2012b; Lin *et al.*, 2013). However, we
304 observed a more robust reduction of PVT-projecting TH-neurons in the NTS (-34.2%)
305 compared to the LC (-15.1%) (**Figure 1C, D**). No differences were observed in the
306 A1 area of the hindbrain (**Figure 1C, D**) as well as in the hypothalamus (**Suppl.**
307 **Figure 1B**, <https://doi.org/10.6084/m9.figshare.19683228.v1>).

308 Then we investigated whether the reduction in local TH-afferents was followed by the
309 modulation of PVT-neurons activity. Since the PVT shows higher activity during
310 wakefulness (Ren *et al.*, 2018), mice were perfused 1h before the onset of the dark
311 phase (spontaneous feeding period) and at basal conditions. Using cFos as a

312 molecular proxy of cellular activity, we observed a significant increase in cFos-
313 positive cells in the PVT of 6-OHDA^{PVT} compared to Sham^{PVT} mice (**Figure 1E, F**).
314 This set of results suggests that a subset of hindbrain CA inputs (hindbrainTH→PVT
315 projections) may serve as modulators of PVT-neurons activity.

316

317 **Catecholaminergic inputs to the PVT contribute to novelty-induced hypophagia**

318 Following 3-4 weeks from 6-OHDA microinjections, no major differences in body
319 weight were detected in 6-OHDA^{PVT} compared to Sham^{PVT} mice (group-housed
320 animals, **Figure 2A**). In order to study the role of PVT catecholaminergic inputs in the
321 regulation of feeding patterns, 6-OHDA^{PVT} and Sham^{PVT} mice were single-housed
322 (**Figure 2B**). Environmental and social isolation, as triggered by single housing,
323 represent behavioral/environmental stress-like allostatic stimuli (Lee *et al.*, 2020,
324 2021) which can trigger a transient reduction of food intake (Takatsu-Coleman *et al.*,
325 2013; Benfato *et al.*, 2022). Interestingly, we observed that 6-OHDA^{PVT} mice were
326 less sensitive to single housing-induced hypophagia compared to Sham^{PVT} mice
327 (**Figure 2C**). This phenotype prompted us to investigate whether catecholaminergic
328 inputs to the PVT were important in driving feeding patterns and metabolic
329 adaptations to exposure to other behavioral/environmental challenges.

330 After 2 weeks of habituation to single-housing, we analyzed the metabolic efficiency
331 of 6-OHDA^{PVT} and Sham^{PVT} mice exposed to a novel environment during two
332 consecutive exposures during the dark period (spontaneous feeding period, **Figure**
333 **2D**). While Sham^{PVT} mice transiently (Exp.1) showed a reduction in food intake
334 during the dark period (**Figure 2E, E¹**), 6-OHDA^{PVT} mice were again less sensitive to
335 novelty-induced hypophagia. No differences in food intake were measured during
336 Exp.2 period between the two groups, indicating a rapid restoration of homeostatic
337 regulations associated to environmental habituation (**Figure 2E, E¹**). This phenotype
338 was not associated to changes in locomotor activity as indicated by the similar
339 patterns of exploration (Exp.1, novelty) and habituation (Exp.2) (**Figure 2F, F¹**). We
340 also measured key whole-body metabolic parameters such as the respiratory
341 exchange ratio (RER, indicative of the energy substrates used, RER≈1 for
342 carbohydrates, RER≈0.7 for lipids), fatty acid oxidation (FAO) and energy
343 expenditure (EE) during the exposure to the novel environment (Exp.1). Compared to
344 Sham^{PVT} mice, 6-OHDA^{PVT} animals showed increased RER (**Figure 2G, G¹**) and
345 decreased FAO (**Figure 2H, H¹**), mirroring the changes in food intake and indicating

346 a shift of energy substrates (carbohydrates and lipids) use during exposure to a novel
347 environment. However, these adaptations did not impact on energy expenditure
348 (**Figure 2I, I¹**), suggesting that nutrient partitioning (Joly-Amado *et al.*, 2012), rather
349 than total energy balance, was affected by the loss of hindbrainTH→PVT fibers.

350 One may wonder whether the absence of novelty-induced hypophagia in 6-OHDA^{PVT}
351 mice may be associated to enhanced perception and/or reward value of food. To
352 investigate this aspect, Sham^{PVT} and 6-OHDA^{PVT} mice were intermittently (1h/day)
353 exposed to high-fat high-sugar (HFHS) diet during two consecutive days. No
354 differences in HFHS food intake were observed between groups (**Suppl. Figure 2A**,
355 <https://doi.org/10.6084/m9.figshare.19683228.v1>), suggesting intact food palatability,
356 perception and preference. These results suggest that hindbrainTH→PVT fibers
357 represent an important node for the integration of homeostatic regulations.

358 Exposure to novel environments can lead to the occurrence of anxiogenic traits and
359 novelty-triggered thermogenic adaptations (Lecorps *et al.*, 2016) which may impact
360 on, and therefore confound, the mechanisms underlying feeding strategies. Thus, we
361 performed an open field test (OF, **Figure 3A**) to evaluate both anxiety and
362 thermogenic adaptations. We observed no significant differences in anxiety-like
363 parameters between Sham^{PVT} and 6-OHDA^{PVT} animals (**Figure 3B-F**). Moreover,
364 both groups showed similar thermogenic enhancements in the brown adipose tissue
365 (BAT), the lower back and the tail (**Figure 3G-J**). These results indicate that PVT-
366 projecting TH-afferents modulate feeding patterns and metabolic efficiency
367 independently from affective (anxiety) and thermogenic adaptations.

368 Feeding patterns and metabolic efficiency highly depend on circadian rhythms and
369 strong functional interactions exist between circadian rhythms, feeding and energy
370 balance (Challet, 2019). Moreover, the PVT, which is bidirectionally connected with
371 the suprachiasmatic nucleus (SCN) (Peng & Bentivoglio, 2004; Colavito *et al.*, 2015),
372 has been pointed as a contributor to circadian cycles and its activity varies depending
373 on active/inactive phases (Colavito *et al.*, 2015; Kirouac, 2015). Thus, we decided to
374 investigate whether PVT catecholaminergic inputs participated to the adaptive
375 metabolic strategies occurring during circadian challenges by inverting the light/dark
376 cycle (**Figure 4A**). First, before inverting the light/dark cycle, we confirmed (**Figure 2**)
377 that exposure to the new environment was associated to reduced novelty-induced
378 hypophagia in 6-OHDA^{PVT} compared to Sham^{PVT} mice (**Suppl. Figure 3A, B**,
379 <https://doi.org/10.6084/m9.figshare.19683228.v1>). Then, after habituation, light/dark

380 cycles were inverted. When measuring food intake, we observed that both
381 experimental groups rapidly shifted and adapted toward the new light/dark schedule
382 (average of first 2 days of standard and inverted cycles) (**Figure 4B, B¹**). In fact,
383 despite the adaptive shift (**Figure 4B, B¹**), no differences were observed in the
384 cumulative food intake (**Figure 4C**). Moreover, we also detected a similar pattern of
385 circadian adaptation in the EE profile of both groups (**Figure 4D, D¹**), with an
386 increased EE in the 7h-19h inverted period (iDark) and a decreased EE in the 19h-7h
387 inverted period (iLight) (**Figure 4E, E¹**). Interestingly, we found a significant
388 difference in FAO and RER. In particular, while Sham^{PVT} animals rapidly adapted to
389 the inverted light/dark cycle (**Figure 4F**), 6-OHDA^{PVT} mice did not show significant
390 changes in FAO during the 7h-19h inverted period (iDark) (**Figure 4F¹, G**), whereas
391 both groups showed increased FAO during the 19h-7h inverted period (iLight)
392 (**Figure 4G¹**). In line with this shift in energy substrates partitioning, measurements of
393 RER indicated an impaired adjustment of metabolic efficiency during the iDark period
394 (7h-19h) in 6-OHDA^{PVT} mice (**Figure 4H, H¹, I, I¹**).

395 These results suggest that hindbrainTH→PVT inputs, although not involved in the
396 adaptation of food intake to circadian challenges, are important in adjusting
397 peripheral energy substrates utilization (*i.e* lipids and carbohydrates as revealed by
398 RER and FAO) and overall metabolic efficiency.

399

400 **Catecholaminergic inputs to the PVT contribute to feeding under physiological** 401 **and metabolic challenges**

402 Next, we wondered whether hindbrainTH→PVT inputs guided feeding following
403 physiological and metabolic stressors. First, to mimic a conflict between hunger and
404 environmental stress, we decided to study food intake in overnight fasted mice in a
405 novelty-induced hypophagia test. After an overnight fasting, both grouped showed a
406 similar reduction in body weight and plasma glucose levels (**Suppl. Figure 4A, B**,
407 <https://doi.org/10.6084/m9.figshare.19683228.v1>). Then mice underwent the novelty-
408 suppressed feeding (NSF) test (**Figure 5A**). Sham^{PVT} and 6-OHDA^{PVT} mice showed
409 similar latency to eat (**Figure 5B**), with a significant difference in food intake which
410 was higher in 6-OHDA^{PVT} mice (**Figure 5C, D**). The NSF test (latency to eat) is
411 mainly used to assess anxiety- and depressive-like phenotypes. Therefore, our
412 results suggest that the increased food intake observed following PVT
413 catecholaminergic ablation may not be confounded by potential alterations triggered

414 by anxiety. This is in line with our above-mentioned observations using the open field
415 test (**Figure 3A-F**).

416 Then, we used an acute restraint (immobilization) paradigm which is known to alter
417 metabolism and food intake (Rybkin *et al.*, 1997; Vallès *et al.*, 2000; Rabasa &
418 Dickson, 2016). Sham^{PVT} and 6-OHDA^{PVT} mice underwent a 30 min acute restraint
419 and food intake was measured during the dark period. Although both groups showed
420 a significant reduction in food intake (**Figure 5E**), stress-induced hypophagia was
421 significantly more pronounced in Sham^{PVT} compared to 6-OHDA^{PVT} mice (**Figure**
422 **5E**).

423 To further investigate the role of hindbrainTH→PVT inputs in scaling feeding, we used
424 metabolic stressors to modulate food intake. First, Sham^{PVT} and 6-OHDA^{PVT} mice
425 were administered with 2-deoxy-d-glucose (2-DG) which, in virtue of its glucoprivic
426 effects (neuroglucopenia), elicits food consumption as well as the typical glucose
427 counterregulatory response (CRR) (Pénicaud *et al.*, 1986; Lewis *et al.*, 2006).
428 Moreover, PVT-neurons are highly sensitive to glucoprivation (Labouèbe *et al.*,
429 2016). In this conditions, 6-OHDA^{PVT} mice consumed more chow food than Sham^{PVT}
430 mice (**Figure 6A**), even though the magnitude of the glucose excursion as
431 counterregulatory response was similar between groups (**Figure 6B**). This result
432 suggests that hindbrainTH→PVT projections are required to fully express feeding
433 adaptations to glucoprivic conditions but are dispensable for the autonomic control of
434 glycogen breakdown and glucose production in CRR. In the same line, glucose
435 clearance dynamics during an oral glucose tolerance test (OGTT, **Figure 6C**) or an
436 insulin tolerance test (ITT, **Figure 6D**) were similar between sham and 6-OHDA^{PVT}
437 mice, indicating that glucose metabolism and insulin sensitivity remained unaltered
438 following the loss of hindbrainTH→PVT inputs.

439 Second, we performed a fasting-refeeding test to mimic a negative energy balance
440 (food deprivation). In line with the NSF test (**Figure 5C, D**), after an overnight fasting
441 and a similar loss of body weight (**Suppl. Figure 4C**,
442 <https://doi.org/10.6084/m9.figshare.19683228.v1>), both experimental groups showed
443 an enhanced food intake with 6-OHDA^{PVT} mice consuming more food than Sham^{PVT}
444 mice (**Figure 6E**). Third, we also decided to measure drinking and food intake in
445 overnight water-deprived animals. Both groups showed again a similar decrease in
446 body weight (**Suppl. Figure 4D**, <https://doi.org/10.6084/m9.figshare.19683228.v1>).
447 After deprivation, mice were exposed to water. While no differences were observed

448 in drinking behavior (**Figure 6F**), 6-OHDA^{PVT} mice again consumed more food than
449 Sham^{PVT} mice (**Figure 6G**). These results suggest that hindbrainTH→PVT inputs
450 scale food intake also following physiological and metabolic stressors.

451 In order to assess whether orexigenic signals without metabolic challenges also
452 required an intact PVT catecholaminergic transmission, we administered ghrelin in
453 fed mice. As shown in **Figure 6H**, ghrelin similarly induced an increase in food intake
454 in both groups, thereby indicating that canonical orexigenic circuits are not altered.

455

456 **Reduced catecholaminergic transmission in the PVT promotes the activation of** 457 **hypothalamic regions**

458 The above-mentioned results point to hindbrainTH→PVT afferents as major actors in
459 scaling food intake and metabolic efficiency. Since these homeostatic functions
460 highly depend on the hypothalamus, classically described as the master regulator of
461 energy balance (Dietrich & Horvath, 2013; Timper & Brüning, 2017), we decided to
462 study whether 6-OHDA^{PVT} mice were characterized by an altered basal activity
463 (cFos-positive cells) of key hypothalamic regions such as the dorsomedial
464 hypothalamus (DMH), the ventromedial hypothalamus (VMH), the lateral
465 hypothalamus (LH) and the arcuate nucleus (Arc). As for **Figure 1**, mice were
466 perfused 1h before the onset of the dark phase. Interestingly, in 6-OHDA^{PVT} mice we
467 observed an increase in cFos-positive cells specifically in the DMH and LH (**Figure**
468 **7A-C**) compared to Sham^{PVT} mice, whereas no differences were detected in the VMH
469 and Arc (**Figure 7A, D, E**).

470 In order to see whether PVT-neurons may potentially modulate hypothalamic
471 functions by directly projecting to the DMH and LH, we microinjected an AAV9-CAG-
472 TdTomato virus in the PVT (**Figure 7F, G**). As shown in **Figure 7G**, we observed
473 direct PVT→DMH and PVT→LH projections. These results suggest that the
474 increased activity of PVT-neurons following catecholamines depletion (**Figure 1**) may
475 impact, directly (**Figure 7G**) and/or indirectly (polysynaptic circuits), on the regulatory
476 activity of the hypothalamus which may ultimately result in the modulation of food
477 intake and metabolic efficiency.

478 Discussion

479

480 The regulation of food intake represents one of the most complex biological
481 functions. Pivotal for adaptation and survival, the regulatory processes underlying
482 feeding are constantly shaped by signals reflecting/sensing physiological
483 adjustments. In virtue of their heterogeneity (exteroceptive vs interoceptive sources),
484 stress-like allostatic stimuli are indeed powerful modulators of food intake, feeding
485 habits and metabolic adaptations.

486 In this study, we report that hindbrain catecholaminergic (putative noradrenergic)
487 inputs to the PVT play a key role in modulating food intake and metabolic efficiency
488 in stress-related contexts. In fact, permanent ablation of TH-afferents to the PVT
489 resulted in enhanced food intake, adjusted metabolic efficiency and nutrient
490 partitioning whenever environmental, behavioral, physiological and/or metabolic
491 (acute/transient) stressors were introduced as dependent variables of feeding
492 behaviors. In particular, 6-OHDA^{PVT} mice were resistant or less sensitive to
493 environmental and behavioral stress-induced hypophagia and showed enhanced
494 feeding patterns following physiological and metabolic challenges. The different
495 nature of stressors used in this study highlights the highly conserved role of CA
496 inputs to the PVT in readily scaling feeding and metabolic adaptations. Moreover,
497 beyond the impact on feeding and metabolic efficiency, it is important to mention that
498 stressors-elicited homeostatic adaptations such as energy expenditure and
499 thermogenesis did not depend on PVT CA inputs, suggesting a functional tropism of
500 hindbrainTH→PVT circuits toward food intake on one hand and peripheral nutrient
501 partitioning on the other. This is relevant since previous studies have suggested that
502 PVT-neurons, by facilitating hypothalamic-pituitary-adrenal (HPA) responses
503 (Bhatnagar *et al.*, 2000), may contribute to the regulation of core temperature
504 rhythms as well as body weight gain in chronically stressed rats (Bhatnagar &
505 Dallman, 1999). Whether distinct PVT networks (inputs/outputs) are differently
506 engaged by acute vs chronic stressors on the regulation of body hemostasis will
507 deserve in-depth investigations. Overall, these results indicate that the PVT, a key
508 node of the limbic circuitry (Barson *et al.*, 2020), contributes to the elaboration of
509 food-related decisions and strategies by integrating, among others, also
510 catecholaminergic information. In addition, our results provide new evidence for the
511 existence of distinct, but converging, hindbrain CA inputs (a subset of NTSTH- and

512 LCTH-neurons) capable of gating food-related homeostatic adaptations under
513 transient stress-like allostatic stimuli.

514 Surprisingly, we found that the NTS represented one of the major sources of TH-
515 positive projections to the PVT. In fact, local microinjection of 6-OHDA resulted in a
516 significant reduction of TH-expressing neurons in the NTS and to a lesser extent in
517 the LC, sparing CA neurons in the medulla (A1 area) and the hypothalamus, the
518 latter known to send only minor scattered projections to the PVT (Wang *et al.*,
519 2021*b*). Although to our knowledge no other studies have functionally assessed this
520 NTSTH→PVT connection, the impact of 6-OHDA^{PVT} on NTSTH-neurons is in line with
521 the presence of a dense plexus of PVT-reaching TH fibers when fluorescent
522 recombinant markers are directly microinjected in the NTS of *Th-Cre* animals (Aklan
523 *et al.*, 2020) as well as with a recent retrograde viral study identifying a subset of
524 NTSTH-neurons projecting to the PVT (Kirouac *et al.*, 2022). This evidence is of
525 paramount importance since NTS and LC catecholaminergic neurons, by converging
526 onto the PVT, may synergistically modulate feeding patterns and metabolic efficiency
527 in stressogenic contexts. In fact, NTSTH- and LCTH-neurons are well-known to
528 modulate food intake and stress/novelty, respectively (McCall *et al.*, 2015; Roman *et*
529 *al.*, 2016; Takeuchi *et al.*, 2016).

530 Recent studies have shown that activation of CA-releasing NTS^{DBH/TH}-neurons may
531 result in a reduction (Roman *et al.*, 2016; Chen *et al.*, 2020) as well as in an increase
532 (Aklan *et al.*, 2020; Chen *et al.*, 2020) of food intake depending on CA cell types
533 and/or projection sites [parabrachial nucleus (PBN) vs arcuate nucleus (Arc)].
534 Although not directly assessed in our study, our results suggest that NTSTH→PVT
535 projecting neurons may serve as anorexigenic stimuli since their ablation enhances
536 food intake under stress-related contexts. Indeed, it may be legitimately argued that
537 the use of local microinjections of 6-OHDA may result in the degeneration of LCTH-
538 and NTSTH-neurons projecting to the PVT but eventually to also other brain regions.
539 However, loss of hindbrainTH neurons projecting to the medial hypothalamus resulted
540 in a loss of glucoprivation-induced feeding (Fraley & Ritter, 2003; Hudson & Ritter,
541 2004), while in our study we show an increased food consumption under glucoprivic
542 conditions when hindbrainTH→PVT projections were ablated. Moreover, opto-
543 activation of NTSTH→Arc projections leads to an increase in food intake (Aklan *et al.*,
544 2020), whereas in our case enhanced food intake was elicited by the absence of
545 hindbrainTH→PVT projections. These effects may substantiate the functional

546 selectivity of hindbrainTH→PVT projections in the adaptive responses of feeding,
547 metabolic efficiency and nutrient partitioning to stress-related contexts. Indeed, future
548 investigations using projection-specific optogenetics and/or chemogenetics may
549 definitely help in dissecting out the distinct and, most importantly, synergistic roles of
550 NTSTH→PVT and LCTH→PVT transmissions in guiding the tight interaction between
551 food intake, metabolism and stress-like allostatic stimuli.

552 Moreover, we observed that deletion of hindbrainTH→PVT inputs led to an increase in
553 PVT-cells activity (cFos), suggesting that catecholamines may act, directly and/or
554 indirectly, as negative modulators onto PVT-neurons. At first, this is surprising and
555 counterintuitive since *ex vivo* bath-applications of DA (precursor of NE) or NE, which
556 can be synaptically co-released from CA terminals (Smith & Greene, 2012;
557 Kempadoo *et al.*, 2016), lead to disinhibition [DA, (Beas *et al.*, 2018)] or activation
558 [NE, (Wang *et al.*, 2021*b*)] of PVT-neurons. However, it should be mentioned that
559 mid-posterior PVT-neurons express DA D2 and D3 receptors (Rieck *et al.*, 2004;
560 Clark *et al.*, 2017; Beas *et al.*, 2018; Gao *et al.*, 2020) as well as NE receptors such
561 as the $\alpha 1$, $\alpha 2$, $\beta 1$ and $\beta 2$ receptors (Rainbow *et al.*, 1984; Pieribone *et al.*, 1994;
562 Rosin *et al.*, 1996). Indeed, (i) how this variety of G-protein-coupled receptors (G_i -,
563 G_s -, G_q - and β -arrestin-coupled receptors) mechanistically contribute to the overall
564 modulation of PVT-neurons and (ii) whether 6-OHDA-induced TH deletion
565 reorganizes the expression of the above-mentioned CA receptors in the PVT require
566 future investigations. Although our results cannot distinguish between the functional
567 roles of distinct catecholamines onto their associated multiple receptors located onto
568 PVT-neurons, it is worth to mention that the PVT does not receive pure DA-fibers
569 from the midbrain (SNc and VTA) (Li *et al.*, 2014; Papathanou *et al.*, 2019) and that
570 direct 6-OHDA-induced LCTH-neurons loss was associated to an increased
571 expression of Gq-coupled $\alpha 1$ receptor in the thalamus (Szot *et al.*, 2012*a*) which may
572 explain, at least in part, the increase in PVT cFos-neurons.

573 The enhanced activation of PVT-neurons in 6-OHDA^{PVT} mice and the associated
574 feeding behaviors are in line with reports showing that stressors as well as hunger
575 are able to activate PVT-neurons (Bubser & Deutch, 1999; Beas *et al.*, 2018; Hua *et al.*,
576 2018). In addition, our results are also in line with a recent report showing that
577 activation of PVT-neurons by oxytocin was efficient in suppressing stress-induced
578 hypophagia (Barrett *et al.*, 2021). However, it is worth to mention that satietogenic

579 signals are also able to activate PVT-neurons (Ong *et al.*, 2017), therefore indicating
580 that PVT excitatory (glutamate) neurons may be actually segregated into several cell
581 types with distinct neurochemical, cellular and functional features. This is already
582 supported by the existence of at least two neuronal populations [galanin- and
583 dopamine 2 receptor (D2R)-positive neurons, (Gao *et al.*, 2020)] and, as already
584 suggested by the presence of several neuropeptides in PVT-neurons (Curtis *et al.*,
585 2020), it may not be hazardous to hypothesize that future cell type-specific
586 transcriptomic analyses will reveal new sub-families and clusters.

587 The homeostatic processes underlying food intake, energy balance and metabolic
588 efficiency strongly depend on the activity of the hypothalamus (Dietrich & Horvath,
589 2013; Timper & Brüning, 2017). We observed that depletion of TH-afferents to the
590 PVT resulted not only in the activation of PVT-neurons but also in the concomitant
591 activation of hypothalamic regions, notably the lateral (LH) and the dorsomedial
592 (DMH) hypothalamus. Indeed, activation of LH and DMH cell types has been shown
593 to promote feeding (Jennings *et al.*, 2015; Navarro *et al.*, 2016; Otgon-Uul *et al.*,
594 2016; Jeong *et al.*, 2017) even following anxiogenic environmental cues (Cassidy *et al.*,
595 2019). Although we cannot rule out yet whether and how the adaptive activation
596 of PVT-neurons following TH deletion may be responsible for the direct activation of
597 LH and DMH regions, it is interesting to note that PVT excitatory (glutamate) neurons
598 also project to the hypothalamus (Engelke *et al.*, 2021; Li *et al.*, 2021), therefore
599 potentially modulating feeding and energy homeostasis. This is also supported by our
600 viral tracing strategy which revealed direct PVT→DMH/LH projections. However, we
601 cannot formally exclude that the partial loss of hindbrain TH-neurons may impact on
602 the hypothalamic activity in virtue of other circuits (hindbrainTH→hypothalamus and/or
603 hindbrainTH→PBN→hypothalamus paths). Indeed, while the existence of a
604 hypothalamus→PVT→accumbal circuit seems critical for behavioral adaptations
605 (Betley *et al.*, 2013; Zhang & van den Pol, 2017; Otis *et al.*, 2019; Meffre *et al.*, 2019;
606 Zhang *et al.*, 2020; Iglesias & Flagel, 2021; Engelke *et al.*, 2021), our results,
607 together with previous and recent literature (Otake *et al.*, 1994; Ong *et al.*, 2017;
608 Beas *et al.*, 2018; Sofia Beas *et al.*, 2020; Li *et al.*, 2021), also suggest a
609 hindbrain→PVT→hypothalamus path that may regulate homeostatic functions
610 requiring the integration of exteroceptive and interoceptive signals.

611 In conclusion, the PVT has been classically positioned as a functional node of the
612 limbic circuit (Barson *et al.*, 2020). Only recently the hypothesis of the PVT as a

613 homeostatic relay has been proposed (Penzo & Gao, 2021). Altogether, our results
614 support the working hypothesis according to which the PVT, through its afferent
615 connections with NTSTH- and LCTH-neurons, may represent a functional interface
616 between homeostatic and emotional states, thereby leading to allostatic adaptations.
617 This study, besides highlighting the existence of a dual hindbrain-to-thalamus
618 connection, (i) provides new evidence to better understand the dynamic processes
619 underlying the regulation of food intake and energy metabolism, and (ii) may serve as
620 starting step to explore the functional relationships and comorbidities between
621 psychiatric (stress) and metabolic (anorexia, obesity, binge eating) disorders.

622 **Acknowledgments**

623 We thank Olja Kacanski for administrative support; Isabelle Le Parco, Ludovic
624 Maingault, Angélique Dauvin, Aurélie Djemat, Florianne Michel and Daniel Quintas
625 for animals' care; Benoit Bertrand for technical help. We acknowledge the *Functional*
626 *and Physiological Exploration platform* (FPE) of the Université de Paris (BFA, UMR
627 8251) and the animal facility Buffon of the Institut Jacques Monod. This work was
628 supported by the Fyssen Foundation, Nutricia Research Foundation, Allen
629 Foundation Inc., *Agence Nationale de la Recherche* (ANR-21-CE14-0021-01),
630 *Fédération pour la Recherche sur le Cerveau* and *Association France Parkinson*,
631 Université Paris Cité and CNRS. G.L. was supported by the China Scholarship
632 Council (CSC) fellowship.

633

634 **Author Contributions**

635 C.D. performed and analyzed most of the experiments. G.L. performed
636 immunofluorescence studies. J.C. performed surgeries. S.L. provided critical
637 feedback. G.G. conceived and supervised the whole project, and wrote the
638 manuscript with contribution from all coauthors.

639

640 **Data availability statement**

641 All data are presented in the manuscript or supplementary information. For Suppl.
642 Figures see <https://doi.org/10.6084/m9.figshare.19683228.v1>.

643

644 **Competing interests**

645 The authors declare no competing interests.

646

647 **References**

- 648 Aklan I, Sayar Atasoy N, Yavuz Y, Ates T, Coban I, Koksalar F, Filiz G, Topcu IC,
649 Oncul M, Dilsiz P, Cebecioglu U, Alp MI, Yilmaz B, Davis DR, Hajdukiewicz K, Saito
650 K, Konopka W, Cui H & Atasoy D (2020). NTS Catecholamine Neurons Mediate
651 Hypoglycemic Hunger via Medial Hypothalamic Feeding Pathways. *Cell Metab* **31**,
652 313-326.e5.
- 653 Arch JRS, Hislop D, Wang SJY & Speakman JR (2006). Some mathematical and
654 technical issues in the measurement and interpretation of open-circuit indirect
655 calorimetry in small animals. *Int J Obes (Lond)* **30**, 1322–1331.
- 656 Barrett LR, Nunez J & Zhang X (2021). Oxytocin activation of paraventricular
657 thalamic neurons promotes feeding motivation to attenuate stress-induced
658 hypophagia. *Neuropsychopharmacology* **46**, 1045–1056.
- 659 Barson JR, Mack NR & Gao W-J (2020). The Paraventricular Nucleus of the
660 Thalamus Is an Important Node in the Emotional Processing Network. *Front Behav*
661 *Neurosci* **14**, 598469.
- 662 Beas BS, Wright BJ, Skirzewski M, Leng Y, Hyun JH, Koita O, Ringelberg N, Kwon
663 H-B, Buonanno A & Penzo MA (2018). The locus coeruleus drives disinhibition in the
664 midline thalamus via a dopaminergic mechanism. *Nat Neurosci* **21**, 963–973.
- 665 Benfato ID, Quintanilha ACS, Henrique JS, Souza MA, Rosário BDA, Beserra Filho
666 JIA, Santos RLO, Ribeiro AM, Le Sueur Maluf L & de Oliveira CAM (2022). Effects of
667 long-term social isolation on central, behavioural and metabolic parameters in
668 middle-aged mice. *Behav Brain Res* **417**, 113630.
- 669 Berland C et al. (2020). Circulating Triglycerides Gate Dopamine-Associated
670 Behaviors through DRD2-Expressing Neurons. *Cell Metab* **31**, 773-790.e11.
- 671 Berland C, Castel J, Terrasi R, Montalban E, Foppen E, Martin C, Muccioli GG,
672 Luquet S & Gangarossa G (2022). Identification of an endocannabinoid gut-brain
673 vagal mechanism controlling food reward and energy homeostasis. *Mol Psychiatry*,
674 DOI: 10.1038/s41380-021-01428-z.
- 675 Betley JN, Cao ZFH, Ritola KD & Sternson SM (2013). Parallel, redundant circuit
676 organization for homeostatic control of feeding behavior. *Cell* **155**, 1337–1350.
- 677 Bhatnagar S & Dallman MF (1999). The paraventricular nucleus of the thalamus
678 alters rhythms in core temperature and energy balance in a state-dependent manner.
679 *Brain Res* **851**, 66–75.
- 680 Bhatnagar S, Viau V, Chu A, Soriano L, Meijer OC & Dallman MF (2000). A

681 cholecystokinin-mediated pathway to the paraventricular thalamus is recruited in
682 chronically stressed rats and regulates hypothalamic-pituitary-adrenal function. *J*
683 *Neurosci* **20**, 5564–5573.

684 Bubser M & Deutch AY (1999). Stress induces Fos expression in neurons of the
685 thalamic paraventricular nucleus that innervate limbic forebrain sites. *Synapse* **32**,
686 13–22.

687 Cassidy RM, Lu Y, Jere M, Tian J-B, Xu Y, Mangieri LR, Felix-Okoroji B, Selever J,
688 Xu Y, Arenkiel BR & Tong Q (2019). A lateral hypothalamus to basal forebrain
689 neurocircuit promotes feeding by suppressing responses to anxiogenic
690 environmental cues. *Sci Adv* **5**, eaav1640.

691 Challet E (2019). The circadian regulation of food intake. *Nat Rev Endocrinol* **15**,
692 393–405.

693 Chen J, Cheng M, Wang L, Zhang L, Xu D, Cao P, Wang F, Herzog H, Song S &
694 Zhan C (2020). A Vagal-NTS Neural Pathway that Stimulates Feeding. *Curr Biol* **30**,
695 3986-3998.e5.

696 Clark AM, Leroy F, Martyniuk KM, Feng W, McManus E, Bailey MR, Javitch JA,
697 Balsam PD & Kellendonk C (2017). Dopamine D2 Receptors in the Paraventricular
698 Thalamus Attenuate Cocaine Locomotor Sensitization. *eNeuro*; DOI:
699 10.1523/ENEURO.0227-17.2017.

700 Colavito V, Tesoriero C, Wirtu AT, Grassi-Zucconi G & Bentivoglio M (2015). Limbic
701 thalamus and state-dependent behavior: The paraventricular nucleus of the thalamic
702 midline as a node in circadian timing and sleep/wake-regulatory networks. *Neurosci*
703 *Biobehav Rev* **54**, 3–17.

704 Curtis GR, Oakes K & Barson JR (2020). Expression and Distribution of
705 Neuropeptide-Expressing Cells Throughout the Rodent Paraventricular Nucleus of
706 the Thalamus. *Front Behav Neurosci* **14**, 634163.

707 Dietrich MO & Horvath TL (2013). Hypothalamic control of energy balance: insights
708 into the role of synaptic plasticity. *Trends Neurosci* **36**, 65–73.

709 Do-Monte FH, Minier-Toribio A, Quiñones-Laracuenta K, Medina-Colón EM & Quirk
710 GJ (2017). Thalamic Regulation of Sucrose Seeking during Unexpected Reward
711 Omission. *Neuron* **94**, 388-400.e4.

712 Do-Monte FH, Quiñones-Laracuenta K & Quirk GJ (2015). A temporal shift in the
713 circuits mediating retrieval of fear memory. *Nature* **519**, 460–463.

714 Engelke DS, Zhang XO, O'Malley JJ, Fernandez-Leon JA, Li S, Kirouac GJ, Beierlein

- 715 M & Do-Monte FH (2021). A hypothalamic-thalamostriatal circuit that controls
716 approach-avoidance conflict in rats. *Nat Commun* **12**, 2517.
- 717 Even PC & Nadkarni NA (2012). Indirect calorimetry in laboratory mice and rats:
718 principles, practical considerations, interpretation and perspectives. *Am J Physiol*
719 *Regul Integr Comp Physiol* **303**, R459-476.
- 720 Fraley GS & Ritter S (2003). Immunolesion of norepinephrine and epinephrine
721 afferents to medial hypothalamus alters basal and 2-deoxy-D-glucose-induced
722 neuropeptide Y and agouti gene-related protein messenger ribonucleic acid
723 expression in the arcuate nucleus. *Endocrinology* **144**, 75–83.
- 724 Gangarossa G, Castell L, Castro L, Tarot P, Veyrunes F, Vincent P, Bertaso F &
725 Valjent E (2019). Contrasting patterns of ERK activation in the tail of the striatum in
726 response to aversive and rewarding signals. *J Neurochem* **151**, 204–226.
- 727 Gangarossa G, Espallergues J, Mailly P, De Bundel D, de Kerchove d'Exaerde A,
728 Hervé D, Girault J-A, Valjent E & Krieger P (2013). Spatial distribution of D1R- and
729 D2R-expressing medium-sized spiny neurons differs along the rostro-caudal axis of
730 the mouse dorsal striatum. *Front Neural Circuits* **7**, 124.
- 731 Gao C, Leng Y, Ma J, Rooke V, Rodriguez-Gonzalez S, Ramakrishnan C, Deisseroth
732 K & Penzo MA (2020). Two genetically, anatomically and functionally distinct cell
733 types segregate across anteroposterior axis of paraventricular thalamus. *Nat*
734 *Neurosci* **23**, 217–228.
- 735 García-Cabezas MA, Martínez-Sánchez P, Sánchez-González MA, Garzón M &
736 Cavada C (2009). Dopamine innervation in the thalamus: monkey versus rat. *Cereb*
737 *Cortex* **19**, 424–434.
- 738 Herzog H (2020). Integrated pathways that control stress and energy homeostasis.
739 *Nat Rev Endocrinol* **16**, 75–76.
- 740 Heydendael W, Sharma K, Iyer V, Luz S, Piel D, Beck S & Bhatnagar S (2011).
741 Orexins/hypocretins act in the posterior paraventricular thalamic nucleus during
742 repeated stress to regulate facilitation to novel stress. *Endocrinology* **152**, 4738–
743 4752.
- 744 Hsu DT, Kirouac GJ, Zubieta J-K & Bhatnagar S (2014). Contributions of the
745 paraventricular thalamic nucleus in the regulation of stress, motivation, and mood.
746 *Front Behav Neurosci* **8**, 73.
- 747 Hua R, Wang X, Chen X, Wang X, Huang P, Li P, Mei W & Li H (2018). Calretinin
748 Neurons in the Midline Thalamus Modulate Starvation-Induced Arousal. *Curr Biol* **28**,

749 3948-3959.e4.

750 Hudson B & Ritter S (2004). Hindbrain catecholamine neurons mediate
751 consummatory responses to glucoprivation. *Physiol Behav* **82**, 241–250.

752 Iglesias AG & Fligel SB (2021). The Paraventricular Thalamus as a Critical Node of
753 Motivated Behavior via the Hypothalamic-Thalamic-Striatal Circuit. *Front Integr*
754 *Neurosci* **15**, 706713.

755 Jennings JH, Ung RL, Resendez SL, Stamatakis AM, Taylor JG, Huang J, Veleta K,
756 Kantak PA, Aita M, Shilling-Scriver K, Ramakrishnan C, Deisseroth K, Otte S &
757 Stuber GD (2015). Visualizing hypothalamic network dynamics for appetitive and
758 consummatory behaviors. *Cell* **160**, 516–527.

759 Jeong JH, Lee DK & Jo Y-H (2017). Cholinergic neurons in the dorsomedial
760 hypothalamus regulate food intake. *Mol Metab* **6**, 306–312.

761 Joly-Amado A, Denis RGP, Castel J, Lacombe A, Cansell C, Rouch C, Kassis N,
762 Dairou J, Cani PD, Ventura-Clapier R, Prola A, Flamment M, Fougère F, Magnan C &
763 Luquet S (2012). Hypothalamic AgRP-neurons control peripheral substrate utilization
764 and nutrient partitioning. *EMBO J* **31**, 4276–4288.

765 Kempadoo KA, Mosharov EV, Choi SJ, Sulzer D & Kandel ER (2016). Dopamine
766 release from the locus coeruleus to the dorsal hippocampus promotes spatial
767 learning and memory. *Proc Natl Acad Sci U S A* **113**, 14835–14840.

768 Kessler S, Labouèbe G, Croizier S, Gaspari S, Tarussio D & Thorens B (2021).
769 Glucokinase neurons of the paraventricular nucleus of the thalamus sense glucose
770 and decrease food consumption. *iScience* **24**, 103122.

771 Kirouac GJ (2015). Placing the paraventricular nucleus of the thalamus within the
772 brain circuits that control behavior. *Neurosci Biobehav Rev* **56**, 315–329.

773 Kirouac GJ, Li S & Li S (2022). Convergence of monosynaptic inputs from neurons in
774 the brainstem and forebrain on parabrachial neurons that project to the
775 paraventricular nucleus of the thalamus. 2022.02.23.481069. Available at:
776 <https://www.biorxiv.org/content/10.1101/2022.02.23.481069v1> [Accessed April 18,
777 2022].

778 Kvetnansky R, Sabban EL & Palkovits M (2009). Catecholaminergic systems in
779 stress: structural and molecular genetic approaches. *Physiol Rev* **89**, 535–606.

780 Labouèbe G, Boutrel B, Tarussio D & Thorens B (2016). Glucose-responsive
781 neurons of the paraventricular thalamus control sucrose-seeking behavior. *Nat*
782 *Neurosci* **19**, 999–1002.

- 783 Lecorps B, Rödel HG & Féron C (2016). Assessment of anxiety in open field and
784 elevated plus maze using infrared thermography. *Physiol Behav* **157**, 209–216.
- 785 Lee J-S, Kang J-Y & Son C-G (2020). A Comparison of Isolation Stress and
786 Unpredictable Chronic Mild Stress for the Establishment of Mouse Models of
787 Depressive Disorder. *Front Behav Neurosci* **14**, 616389.
- 788 Lee J-S, Lee S-B, Kim D-W, Shin N, Jeong S-J, Yang C-H & Son C-G (2021). Social
789 isolation-related depression accelerates ethanol intake via microglia-derived
790 neuroinflammation. *Sci Adv* **7**, eabj3400.
- 791 Lewis SR, Ahmed S, Khaimova E, Israel Y, Singh A, Kandov Y, Kest B & Bodnar RJ
792 (2006). Genetic variance contributes to ingestive processes: a survey of 2-deoxy-D-
793 glucose-induced feeding in eleven inbred mouse strains. *Physiol Behav* **87**, 595–601.
- 794 Li S, Dong X & Kirouac GJ (2021). Extensive divergence of projections to the
795 forebrain from neurons in the paraventricular nucleus of the thalamus. *Brain Struct*
796 *Funct* **226**, 1779–1802.
- 797 Li S, Shi Y & Kirouac GJ (2014). The hypothalamus and periaqueductal gray are the
798 sources of dopamine fibers in the paraventricular nucleus of the thalamus in the rat.
799 *Front Neuroanat* **8**, 136.
- 800 Lin L-H, Moore SA, Jones SY, McGlashon J & Talman WT (2013). Astrocytes in the
801 rat nucleus tractus solitarii are critical for cardiovascular reflex control. *J Neurosci* **33**,
802 18608–18617.
- 803 Maniam J & Morris MJ (2012). The link between stress and feeding behaviour.
804 *Neuropharmacology* **63**, 97–110.
- 805 McCall JG, Al-Hasani R, Siuda ER, Hong DY, Norris AJ, Ford CP & Bruchas MR
806 (2015). CRH Engagement of the Locus Coeruleus Noradrenergic System Mediates
807 Stress-Induced Anxiety. *Neuron* **87**, 605–620.
- 808 Meffre J, Sicre M, Diarra M, Marchessaux F, Paleressompoulle D & Ambroggi F
809 (2019). Orexin in the Posterior Paraventricular Thalamus Mediates Hunger-Related
810 Signals in the Nucleus Accumbens Core. *Curr Biol* **29**, 3298-3306.e4.
- 811 Navarro M, Olney JJ, Burnham NW, Mazzone CM, Lowery-Gionta EG, Pleil KE,
812 Kash TL & Thiele TE (2016). Lateral Hypothalamus GABAergic Neurons Modulate
813 Consummatory Behaviors Regardless of the Caloric Content or Biological Relevance
814 of the Consumed Stimuli. *Neuropsychopharmacology* **41**, 1505–1512.
- 815 Ong ZY, Liu J-J, Pang ZP & Grill HJ (2017). Paraventricular Thalamic Control of
816 Food Intake and Reward: Role of Glucagon-Like Peptide-1 Receptor Signaling.

- 817 *Neuropsychopharmacology* **42**, 2387–2397.
- 818 Otake K, Reis DJ & Ruggiero DA (1994). Afferents to the midline thalamus issue
819 collaterals to the nucleus tractus solitarii: an anatomical basis for thalamic and
820 visceral reflex integration. *J Neurosci* **14**, 5694–5707.
- 821 Otgon-Uul Z, Suyama S, Onodera H & Yada T (2016). Optogenetic activation of
822 leptin- and glucose-regulated GABAergic neurons in dorsomedial hypothalamus
823 promotes food intake via inhibitory synaptic transmission to paraventricular nucleus
824 of hypothalamus. *Mol Metab* **5**, 709–715.
- 825 Otis JM, Namboodiri VMK, Matan AM, Voets ES, Mohorn EP, Kosyk O, McHenry JA,
826 Robinson JE, Resendez SL, Rossi MA & Stuber GD (2017). Prefrontal cortex output
827 circuits guide reward seeking through divergent cue encoding. *Nature* **543**, 103–107.
- 828 Otis JM, Zhu M, Namboodiri VMK, Cook CA, Kosyk O, Matan AM, Ying R,
829 Hashikawa Y, Hashikawa K, Trujillo-Pisanty I, Guo J, Ung RL, Rodriguez-Romaguera
830 J, Anton ES & Stuber GD (2019). Paraventricular Thalamus Projection Neurons
831 Integrate Cortical and Hypothalamic Signals for Cue-Reward Processing. *Neuron*
832 **103**, 423-431.e4.
- 833 Papathanou M, Dumas S, Pettersson H, Olson L & Wallén-Mackenzie Å (2019). Off-
834 Target Effects in Transgenic Mice: Characterization of Dopamine Transporter (DAT)-
835 Cre Transgenic Mouse Lines Exposes Multiple Non-Dopaminergic Neuronal Clusters
836 Available for Selective Targeting within Limbic Neurocircuitry. *eNeuro* **6**,
837 ENEURO.0198-19.2019.
- 838 Peng Z-C & Bentivoglio M (2004). The thalamic paraventricular nucleus relays
839 information from the suprachiasmatic nucleus to the amygdala: a combined
840 anterograde and retrograde tracing study in the rat at the light and electron
841 microscopic levels. *J Neurocytol* **33**, 101–116.
- 842 Pénicaud L, Thompson DA & Le Magnen J (1986). Effects of 2-deoxy-D-glucose on
843 food and water intake and body temperature in rats. *Physiol Behav* **36**, 431–435.
- 844 Penzo MA & Gao C (2021). The paraventricular nucleus of the thalamus: an
845 integrative node underlying homeostatic behavior. *Trends Neurosci* **44**, 538–549.
- 846 Penzo MA, Robert V, Tucciarone J, De Bundel D, Wang M, Van Aelst L, Darvas M,
847 Parada LF, Palmiter RD, He M, Huang ZJ & Li B (2015). The paraventricular
848 thalamus controls a central amygdala fear circuit. *Nature* **519**, 455–459.
- 849 Pieribone VA, Nicholas AP, Dagerlind A & Hökfelt T (1994). Distribution of alpha 1
850 adrenoceptors in rat brain revealed by in situ hybridization experiments utilizing

- 851 subtype-specific probes. *J Neurosci* **14**, 4252–4268.
- 852 Pliota P, Böhm V, Grössl F, Griessner J, Valenti O, Kraitsy K, Kaczanowska J,
853 Pasiaka M, Lendl T, Deussing JM & Haubensak W (2020). Stress peptides sensitize
854 fear circuitry to promote passive coping. *Mol Psychiatry* **25**, 428–441.
- 855 Qu N, He Y, Wang C, Xu P, Yang Y, Cai X, Liu H, Yu K, Pei Z, Hyseni I, Sun Z,
856 Fukuda M, Li Y, Tian Q & Xu Y (2020). A POMC-originated circuit regulates stress-
857 induced hypophagia, depression, and anhedonia. *Mol Psychiatry* **25**, 1006–1021.
- 858 Rabasa C & Dickson SL (2016). Impact of stress on metabolism and energy balance.
859 *Current Opinion in Behavioral Sciences* **9**, 71–77.
- 860 Rainbow TC, Parsons B & Wolfe BB (1984). Quantitative autoradiography of beta 1-
861 and beta 2-adrenergic receptors in rat brain. *Proc Natl Acad Sci U S A* **81**, 1585–
862 1589.
- 863 Ren S et al. (2018). The paraventricular thalamus is a critical thalamic area for
864 wakefulness. *Science* **362**, 429–434.
- 865 Rieck RW, Ansari MS, Whetsell WO, Deutch AY & Kessler RM (2004). Distribution of
866 dopamine D2-like receptors in the human thalamus: autoradiographic and PET
867 studies. *Neuropsychopharmacology* **29**, 362–372.
- 868 Roman CW, Derkach VA & Palmiter RD (2016). Genetically and functionally defined
869 NTS to PBN brain circuits mediating anorexia. *Nat Commun* **7**, 11905.
- 870 Rosin DL, Talley EM, Lee A, Stornetta RL, Gaylinn BD, Guyenet PG & Lynch KR
871 (1996). Distribution of alpha 2C-adrenergic receptor-like immunoreactivity in the rat
872 central nervous system. *J Comp Neurol* **372**, 135–165.
- 873 Rybkin II, Zhou Y, Volaufova J, Smagin GN, Ryan DH & Harris RB (1997). Effect of
874 restraint stress on food intake and body weight is determined by time of day. *Am J*
875 *Physiol* **273**, R1612-1622.
- 876 Schroeter S, Apparsundaram S, Wiley RG, Miner LH, Sesack SR & Blakely RD
877 (2000). Immunolocalization of the cocaine- and antidepressant-sensitive I-
878 norepinephrine transporter. *J Comp Neurol* **420**, 211–232.
- 879 Smith CC & Greene RW (2012). CNS dopamine transmission mediated by
880 noradrenergic innervation. *J Neurosci* **32**, 6072–6080.
- 881 Sofia Beas B, Gu X, Leng Y, Koita O, Rodriguez-Gonzalez S, Kindel M, Matikainen-
882 Ankney BA, Larsen RS, Kravitz AV, Hoon MA & Penzo MA (2020). A ventrolateral
883 medulla-midline thalamic circuit for hypoglycemic feeding. *Nat Commun* **11**, 6218.
- 884 Sweeney P & Yang Y (2017). Neural Circuit Mechanisms Underlying Emotional

- 885 Regulation of Homeostatic Feeding. *Trends Endocrinol Metab* **28**, 437–448.
- 886 Szot P, Franklin A, Sikkema C, Wilkinson CW & Raskind MA (2012a). Sequential
887 Loss of LC Noradrenergic and Dopaminergic Neurons Results in a Correlation of
888 Dopaminergic Neuronal Number to Striatal Dopamine Concentration. *Front*
889 *Pharmacol* **3**, 184.
- 890 Szot P, Knight L, Franklin A, Sikkema C, Foster S, Wilkinson CW, White SS &
891 Raskind MA (2012b). Lesioning noradrenergic neurons of the locus coeruleus in
892 C57Bl/6 mice with unilateral 6-hydroxydopamine injection, to assess molecular,
893 electrophysiological and biochemical changes in noradrenergic signaling.
894 *Neuroscience* **216**, 143–157.
- 895 Takatsu-Coleman AL, Patti CL, Zanin KA, Zager A, Carvalho RC, Borçoi AR, Ceccon
896 LMB, Berro LF, Tufik S, Andersen ML & Frussa-Filho R (2013). Short-term social
897 isolation induces depressive-like behaviour and reinstates the retrieval of an aversive
898 task: mood-congruent memory in male mice? *J Psychiatry Neurosci* **38**, 259–268.
- 899 Takeuchi T, Duszkiwicz AJ, Sonneborn A, Spooner PA, Yamasaki M, Watanabe M,
900 Smith CC, Fernández G, Deisseroth K, Greene RW & Morris RGM (2016). Locus
901 coeruleus and dopaminergic consolidation of everyday memory. *Nature* **537**, 357–
902 362.
- 903 Timper K & Brüning JC (2017). Hypothalamic circuits regulating appetite and energy
904 homeostasis: pathways to obesity. *Dis Model Mech* **10**, 679–689.
- 905 Ulrich-Lai YM, Fulton S, Wilson M, Petrovich G & Rinaman L (2015). Stress
906 exposure, food intake and emotional state. *Stress* **18**, 381–399.
- 907 Valentino RJ & Van Bockstaele E (2008). Convergent regulation of locus coeruleus
908 activity as an adaptive response to stress. *Eur J Pharmacol* **583**, 194–203.
- 909 Valjent E & Gangarossa G (2021). The Tail of the Striatum: From Anatomy to
910 Connectivity and Function. *Trends Neurosci* **44**, 203–214.
- 911 Vallès A, Martí O, García A & Armario A (2000). Single exposure to stressors causes
912 long-lasting, stress-dependent reduction of food intake in rats. *Am J Physiol Regul*
913 *Integr Comp Physiol* **279**, R1138-1144.
- 914 Wang C, Zhou W, He Y, Yang T, Xu P, Yang Y, Cai X, Wang J, Liu H, Yu M, Liang
915 C, Yang T, Liu H, Fukuda M, Tong Q, Wu Q, Sun Z, He Y & Xu Y (2021a). AgRP
916 neurons trigger long-term potentiation and facilitate food seeking. *Transl Psychiatry*
917 **11**, 11.
- 918 Wang Y, Xu L, Liu M-Z, Hu D-D, Fang F, Xu D-J, Zhang R, Hua X-X, Li J-B, Zhang L,

919 Huang L-N & Mu D (2021**b**). Norepinephrine modulates wakefulness via α 1
920 adrenoceptors in paraventricular thalamic nucleus. *iScience* **24**, 103015.
921 Xu Y, Lu Y, Cassidy RM, Mangieri LR, Zhu C, Huang X, Jiang Z, Justice NJ, Xu Y,
922 Arenkiel BR & Tong Q (2019). Identification of a neurocircuit underlying regulation of
923 feeding by stress-related emotional responses. *Nat Commun* **10**, 3446.
924 Zhang C, Kaye JA, Cai Z, Wang Y, Prescott SL & Liberles SD (2021). Area Postrema
925 Cell Types that Mediate Nausea-Associated Behaviors. *Neuron* **109**, 461-472.e5.
926 Zhang J, Chen D, Sweeney P & Yang Y (2020). An excitatory ventromedial
927 hypothalamus to paraventricular thalamus circuit that suppresses food intake. *Nat*
928 *Commun* **11**, 6326.
929 Zhang X & van den Pol AN (2017). Rapid binge-like eating and body weight gain
930 driven by zona incerta GABA neuron activation. *Science* **356**, 853–859.
931

932 **Figure legends**

933

934 **Figure 1: Retrograde ablation of hindbrain catecholaminergic inputs contribute**
935 **to PVT activity. (A)** Drawing represents the microinjection of 6-OHDA or Vehicle
936 (Veh) in the mid-posterior PVT. **(B)** Immunofluorescence detection of tyrosine
937 hydroxylase (TH) within the PVT in Sham^{PVT} and 6-OHDA^{PVT} mice. Scale bar: 150
938 μm . **(C)** Immunofluorescence detection of TH in PVT-projecting hindbrain regions
939 [nucleus tractus solitarius (NTS), area A1 and locus coeruleus (LC)] in Sham^{PVT} and
940 6-OHDA^{PVT} mice. Scale bars: 150 μm . **(D)** Quantification of TH-positive neurons in
941 the NTS, A1 and LC. Statistics: * $p < 0.05$, ** $p < 0.01$, 6-OHDA^{PVT} vs Sham^{PVT} mice.
942 **(E)** Immunofluorescence detection of cFos-positive neurons in the mid-posterior PVT
943 (mPVT and pPVT). Scale bars: 150 μm . **(F)** Quantification of cFos-positive cells in
944 the mid-posterior PVT. Statistics: *** $p < 0.001$, 6-OHDA^{PVT} vs Sham^{PVT} mice. Data are
945 presented as mean \pm SD. For statistical details see **Statistical Summary Table**.

946

947 **Figure 2: HindbrainTH→PVT inputs participate to novelty-induced hypophagia.**
948 **(A)** Body weight of Sham^{PVT} and 6-OHDA^{PVT} mice following 3-4 weeks from 6-OHDA
949 or Veh microinjection in the PVT. **(B)** Experimental design indicating the transition
950 from grouped to singled housing. **(C)** Food intake (g/day and kcal/day) during the first
951 three days of isolation (D1 to D3). Statistics: * $p < 0.05$, ** $p < 0.01$, 6-OHDA^{PVT} vs
952 Sham^{PVT} mice. **(D)** Investigation of food intake and metabolic efficiency using
953 metabolic cages during two consecutive exposures to a novel environment. **(E)** Food
954 intake during the dark phase (spontaneous eating) in Sham^{PVT} and 6-OHDA^{PVT} mice
955 during two consecutive exposures to a novel environment. **(E¹)** Cumulative food
956 intake. Statistics: *** $p < 0.01$, Sham^{E2} vs Sham^{E1}, ## $p < 0.01$, 6-OHDA^{E1} vs Sham^{E1}
957 groups. **(F)** Spontaneous locomotor activity (beam breaks, bb) during the dark phase
958 in Sham^{PVT} and 6-OHDA^{PVT} mice during two consecutive exposures to a novel
959 environment. **(F¹)** Cumulative locomotor activity. Statistics: ** $p < 0.01$, Sham^{E2} vs
960 Sham^{E1}; ### $p < 0.001$, 6-OHDA^{E2} vs 6-OHDA^{E1} groups. Note that both experimental
961 groups showed similar degrees of habituation (reduced locomotor activity during the
962 dark period). Measurements of the respiratory exchange ratio (RER, **G**), fatty acid
963 oxidation (FAO, **H**), and energy expenditure (EE, **I**) in Sham^{PVT} and 6-OHDA^{PVT} mice
964 during the first exposure (Exp.1) to a novel environment. **(G¹⁻¹)** Averaged RER,

965 FAO and EE during the dark phase. Statistics: ** $p < 0.01$, 6-OHDA^{E1} vs Sham^{E1}. Data
966 are presented as mean \pm SD. For statistical details see **Statistical Summary Table**.

967

968 **Figure 3: HindbrainTH→PVT inputs do not alter novelty-induced anxiety and**

969 **thermogenesis. (A)** Drawing represents the open field (OF) test. **(B-F)** Parameters

970 measured during a 20 min OF test: total distance, number of entries in the center, %

971 of time in the center, mean exploration visits to the center, distance in the center. **(G)**

972 Infrared thermographic images of animals after the OF test (20 min). **(H-J)**

973 Temperature ($^{\circ}$ C) of the brown adipose tissue (BAT), lower back and tail in Sham^{PVT}

974 and 6-OHDA^{PVT} mice before and after the OF test. Statistics: *** $p < 0.001$, After vs

975 Before OF test (Sham^{PVT} mice); ### $p < 0.001$, After vs Before OF test (6-OHDA^{PVT}

976 mice). No differences were detected between Sham^{PVT} and 6-OHDA^{PVT} mice. Data

977 are presented as mean \pm SD. For statistical details see **Statistical Summary Table**.

978

979 **Figure 4: HindbrainTH→PVT inputs contribute to the circadian adaptation of**

980 **metabolic efficiency. (A)** Drawing indicates the experimental procedure used to

981 study feeding and metabolic adaptations during an inverted cycle (transition from

982 Light-to-Dark to Dark-to-Light). **(B, B¹)** Food intake in Sham^{PVT} **(B)** and 6-OHDA^{PVT}

983 **(B¹)** mice during the standard and inverted cycles. Note how the temporal dynamics

984 of feeding change during the inverted cycle. **(C)** Cumulative food intake in Sham^{PVT}

985 and 6-OHDA^{PVT} mice during the standard and inverted cycles. **(D, D¹)** Temporal

986 dynamics of EE adaptations in Sham^{PVT} **(D)** and 6-OHDA^{PVT} **(D¹)** mice during the

987 standard and inverted cycles. **(E, E¹)** Averaged EE in Sham^{PVT} and 6-OHDA^{PVT} mice

988 according to matched inverted phases (7h-19h, **E**, and 19h-7h, **E¹**). Statistics: ***

989 $p < 0.001$, Inverted vs Standard cycle (Sham^{PVT} mice); ### $p < 0.001$, Inverted vs

990 Standard cycle (6-OHDA^{PVT} mice). **(F, F¹)** Temporal dynamics of FAO adaptations in

991 Sham^{PVT} **(F)** and 6-OHDA^{PVT} **(F¹)** mice during the standard and inverted cycles. **(G,**

992 **G¹)** Averaged FAO in Sham^{PVT} and 6-OHDA^{PVT} mice according to matched inverted

993 phases (7h-19h, **G**, and 19h-7h, **G¹**). Statistics: *** $p < 0.001$, ** $p < 0.01$, Inverted vs

994 Standard cycle (Sham^{PVT} mice); # $p < 0.01$, Inverted vs Standard cycle (6-OHDA^{PVT}

995 mice). **(H, H¹)** Temporal dynamics of RER adaptations in Sham^{PVT} **(H)** and 6-

996 OHDA^{PVT} **(H¹)** mice during the standard and inverted cycles. **(I, I¹)** Averaged RER in

997 Sham^{PVT} and 6-OHDA^{PVT} mice according to matched inverted phases (7h-19h, **I**, and

998 19h-7h, I¹). Statistics: *** p<0.001, ** p<0.01, Inverted vs Standard cycle (Sham^{PVT}
999 mice); ### p<0.01, Inverted vs Standard cycle (6-OHDA^{PVT} mice). Data are presented
1000 as mean ± SD. For statistical details see **Statistical Summary Table**.

1001

1002 **Figure 5: HindbrainTH→PVT inputs scale feeding following physiological**
1003 **stressors. (A)** Drawing represents the novelty-suppressed feeding (NSF) test in
1004 overnight fasted Sham^{PVT} and 6-OHDA^{PVT} mice. **(B)** Latency to eat (first bite) during
1005 the NSF test. **(C, D)** Food intake, total kcal **(C)** and normalized kcal/BW **(D)** during
1006 the NSF test. Statistics: ** p<0.01, 6-OHDA^{PVT} vs Sham^{PVT} mice. **(E)** Food intake in
1007 Sham^{PVT} and 6-OHDA^{PVT} mice after a restraint stress (immobilization). NoR: No
1008 Restraint (control conditions). R: Restraint. Statistics: *** p<0.001, Restraint vs No
1009 Restraint (Sham^{PVT}); ## p<0.01, Restraint vs No Restraint (6-OHDA^{PVT}); \$\$\$ p<0.001,
1010 6-OHDA^{PVT} vs Sham^{PVT} mice (Restraint). Data are presented as mean ± SD. For
1011 statistical details see **Statistical Summary Table**.

1012

1013 **Figure 6: HindbrainTH→PVT inputs scale feeding following metabolic stressors.**
1014 **(A)** Food intake in Sham^{PVT} and 6-OHDA^{PVT} mice administered with 2-DG (500
1015 mg/kg, i.p., neurogluopenia-induced feeding). **(B)** Glucose variation (%) following
1016 administration of 2-DG (0 vs 30 min post administration). Note: neurogluopenia-
1017 induced hyperglycemia is the typical readout of the glucose counterregulatory
1018 response (CRR). **(C, D)** Glucose dynamics during the oral glucose tolerance test
1019 (OGTT, **C**) and the insulin tolerance test (ITT, **D**). No differences were observed
1020 between groups. **(E)** Food intake in overnight fasted Sham^{PVT} and 6-OHDA^{PVT} mice
1021 (refeeding). **(F)** Water intake in overnight water-deprived Sham^{PVT} and 6-OHDA^{PVT}
1022 mice. **(G)** Food intake in overnight water-deprived Sham^{PVT} and 6-OHDA^{PVT} mice. **(H)**
1023 Food intake in Sham^{PVT} and 6-OHDA^{PVT} mice administered with ghrelin (0.5 mg/kg,
1024 i.p., orexigenic response). Statistics: * p<0.05, ** p<0.01, *** p<0.001, 6-OHDA^{PVT} vs
1025 Sham^{PVT} mice. Data are presented as mean ± SD. For statistical details see
1026 **Statistical Summary Table**.

1027

1028 **Figure 7: Deletion of hindbrainTH→PVT inputs increases cFos expression in the**
1029 **hypothalamus. (A)** Immunofluorescence detection of cFos in hypothalamic regions
1030 of Sham^{PVT} and 6-OHDA^{PVT} mice, notably the dorsomedial hypothalamus (DMH), the

1031 lateral hypothalamus (LH), the ventromedial hypothalamus (VMH) and the arcuate
1032 nucleus (Arc). Regions of interest are delineated by white dotted lines. Insets
1033 represent higher magnifications of DMH and LH regions. Scale bars: 500 μm .
1034 Quantification of cFos-positive cells in the DMH (**B**), LH (**C**), VMH (**D**) and Arc (**E**)
1035 regions. Statistics: ** $p < 0.01$, 6-OHDA^{PVT} vs Sham^{PVT} mice. Abbreviations: f (fornix).
1036 (**F**) Drawing indicates the microinjection of AAV9-CAG-TdTomato in the PVT. (**G**)
1037 Immunofluorescence detection of TdTomato in the PVT (injection site), DMH and LH
1038 (projections). Scale bars: 150 μm . Data are presented as mean \pm SD. For statistical
1039 details see **Statistical Summary Table**.

1040

1041 **Suppl. Figure 1: Detection of DAT-positive fibers in the PVT and TH-positive**
1042 **neurons in the hypothalamus following PVT 6-OHDA microinjections. (A)**
1043 Immunofluorescence detection of the dopamine transporter (DAT, red) and DAPI
1044 (blue) in the PVT, tail of the striatum (TS) and central amygdala (CeA). The lack of
1045 DAT-positive fibers in the PVT suggests no direct projections from dopamine-(DAT)-
1046 containing midbrain regions. Scale bar: 150 μm . (**B**) Immunofluorescence detection
1047 of TH (red) and DAPI (blue) in the hypothalamus of Sham^{PVT} and 6-OHDA^{PVT} mice.
1048 Scale bar: 500 μm .

1049

1050 **Suppl. Figure 2: HindbrainTH→PVT inputs dos not alter palatability for HFHS**
1051 **diet. (A)** Food intake in Sham^{PVT} and 6-OHDA^{PVT} mice following time-locked feeding
1052 (1h) of high-fat high-sugar (HFHS) diet during two consecutive days. Statistics: **
1053 $p < 0.01$, Day2 vs Day1 (Sham^{PVT} mice); ### $p < 0.01$, Day2 vs Day1 (6-OHDA^{PVT} mice).
1054 No differences between experimental groups. Data are presented as mean \pm SD. For
1055 statistical details see **Statistical Summary Table**.

1056

1057 **Suppl. Figure 3: Confirmation of sensitivity to novelty-induced hypophagia in**
1058 **Sham^{PVT} and 6-OHDA^{PVT} mice before the inverted cycle. (A)** Cumulative food
1059 intake during the dark phase (spontaneous eating) in Sham^{PVT} and 6-OHDA^{PVT} mice
1060 during the first exposure to a novel environment (calorimetric chambers). (**B**) Total
1061 food intake during the dark phase. Statistics: *** $p < 0.001$, ** $p < 0.01$, 6-OHDA^{PVT} vs
1062 Sham^{PVT} mice. Data are presented as mean \pm SD. For statistical details see
1063 **Statistical Summary Table**.

1064

1065 **Suppl. Figure 4: Effect of fasting and water deprivation in Sham^{PVT} and 6-**
1066 **OHDA^{PVT} mice. (A)** Loss of body weight and **(B)** glucose variations in overnight
1067 fasted animals used for the novelty-suppressed feeding (NSF) test. **(C)** Loss of body
1068 weight in overnight fasted animals before the refeeding schedule. **(D)** Loss of body
1069 weight in overnight water-deprived animals before having access to water and chow
1070 pellets. No differences between experimental groups. Data are presented as mean \pm
1071 SD. For statistical details see **Statistical Summary Table**.

Figure 1

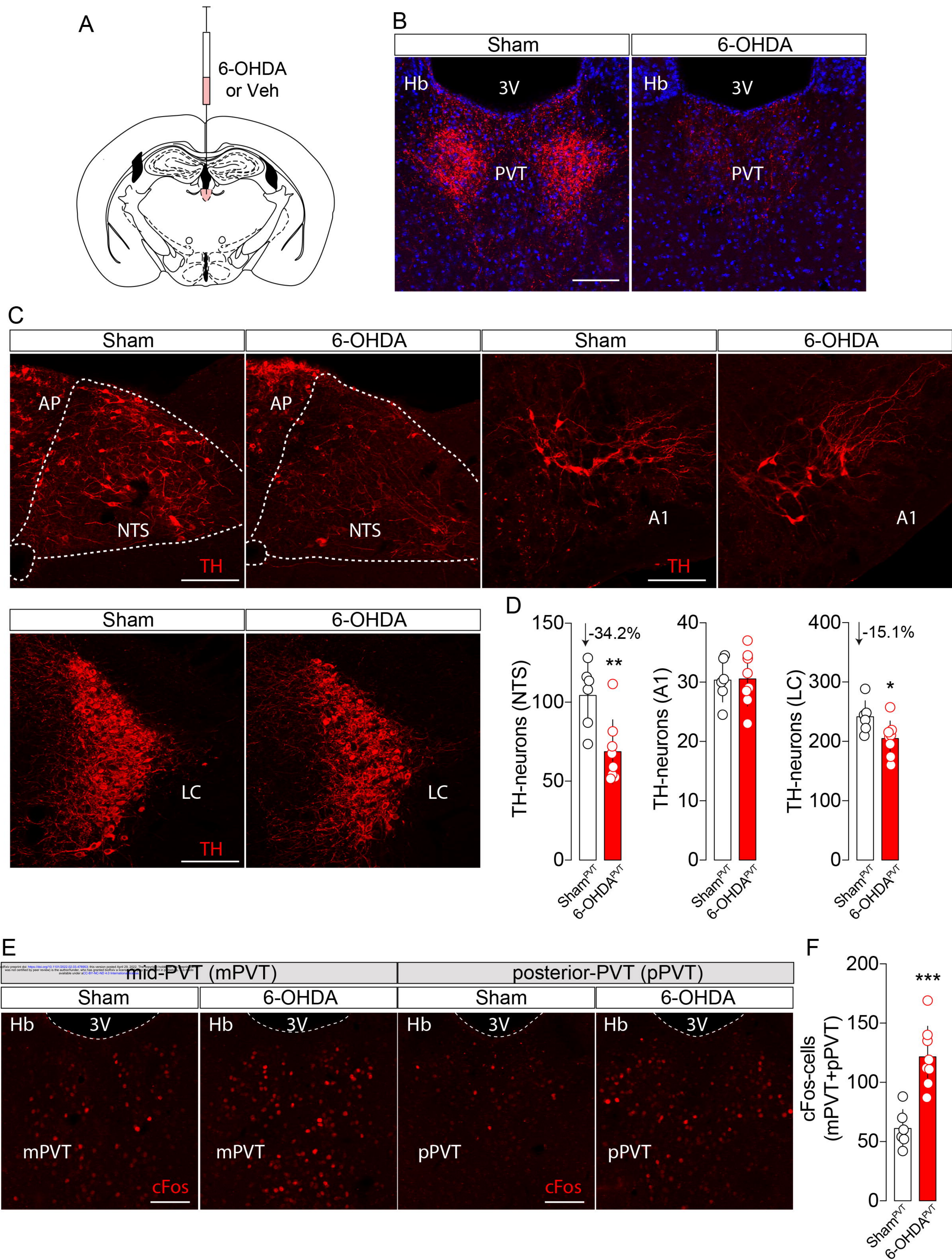


Figure 2

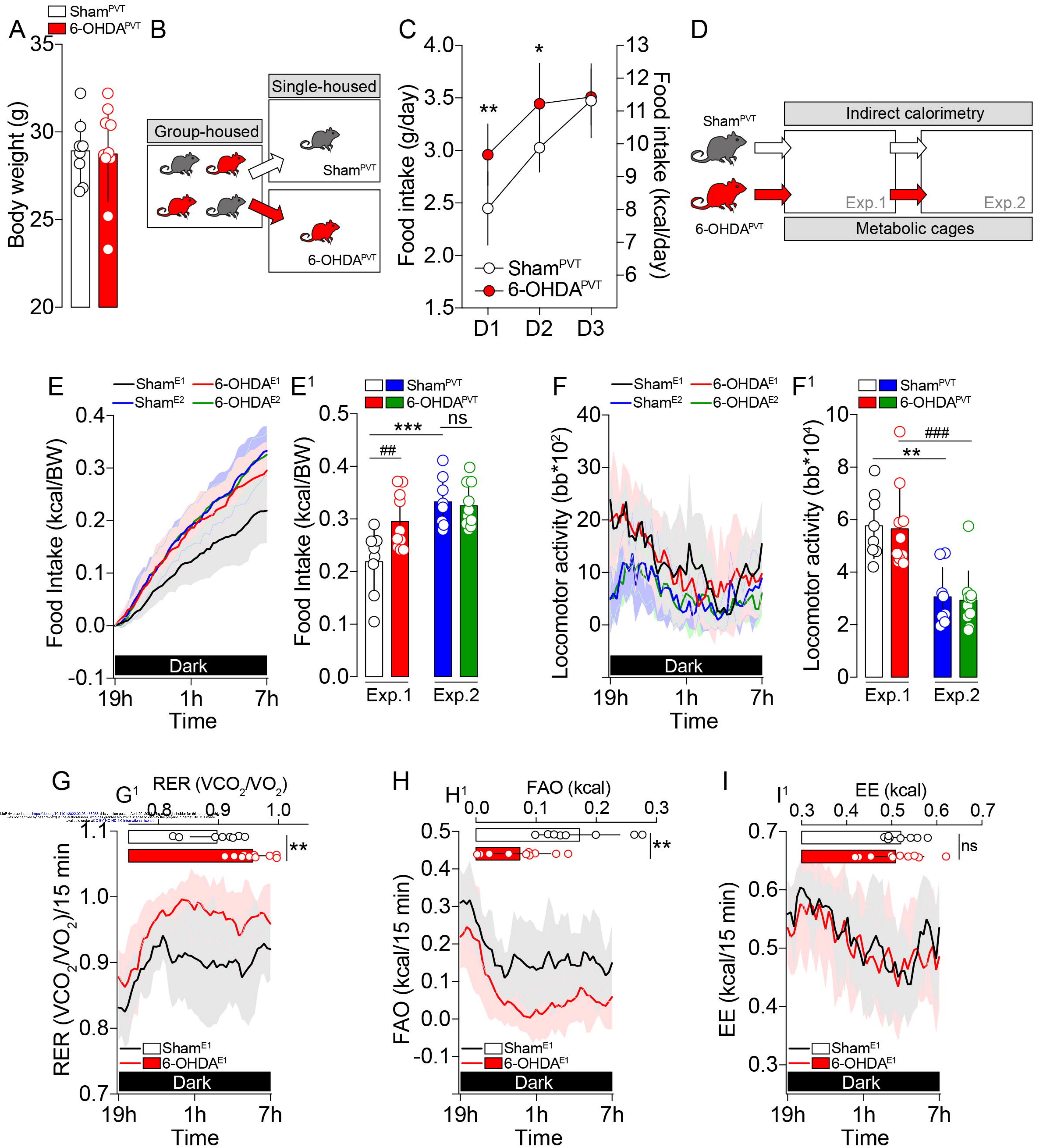


Figure 3

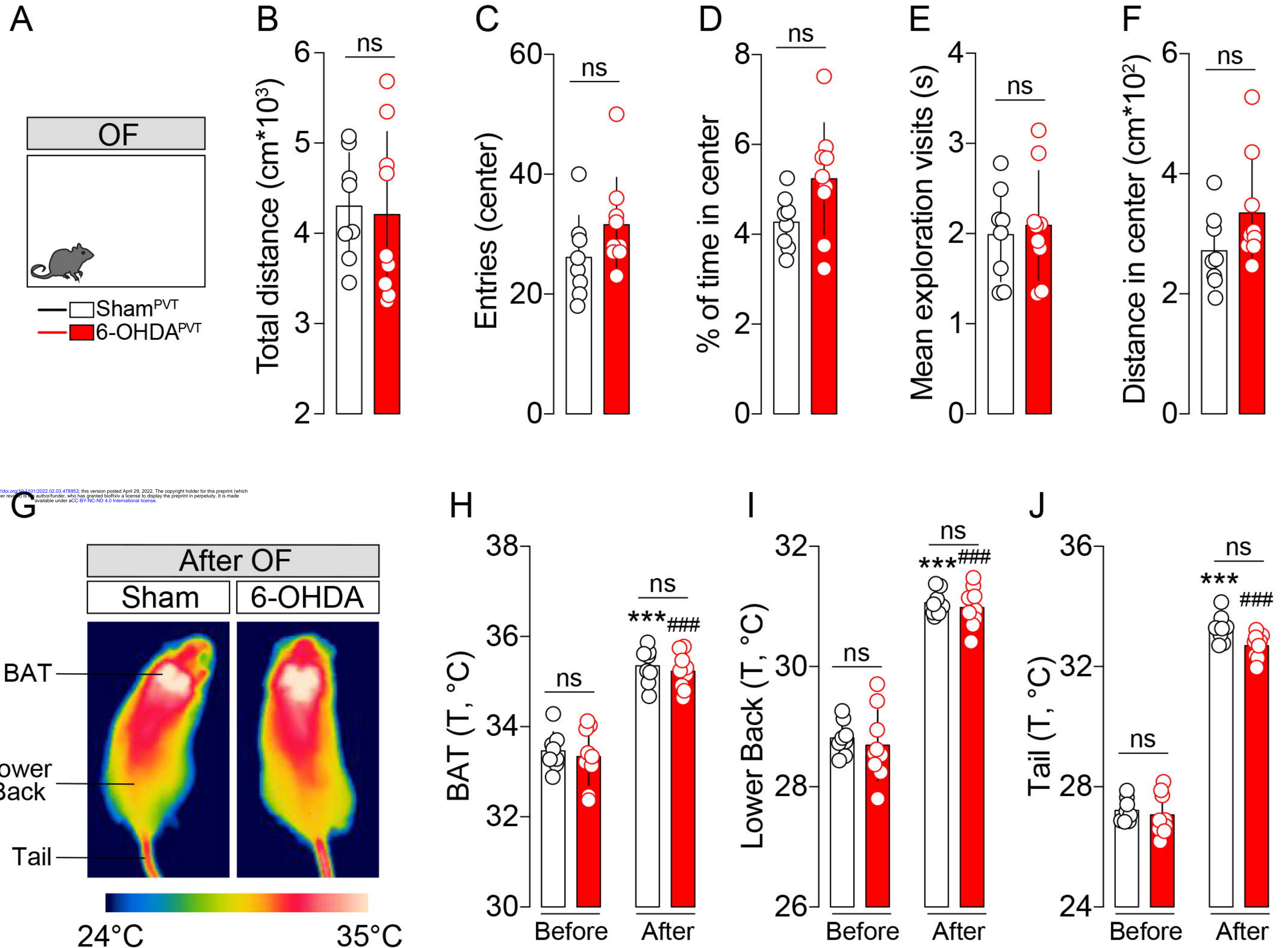


Figure 4

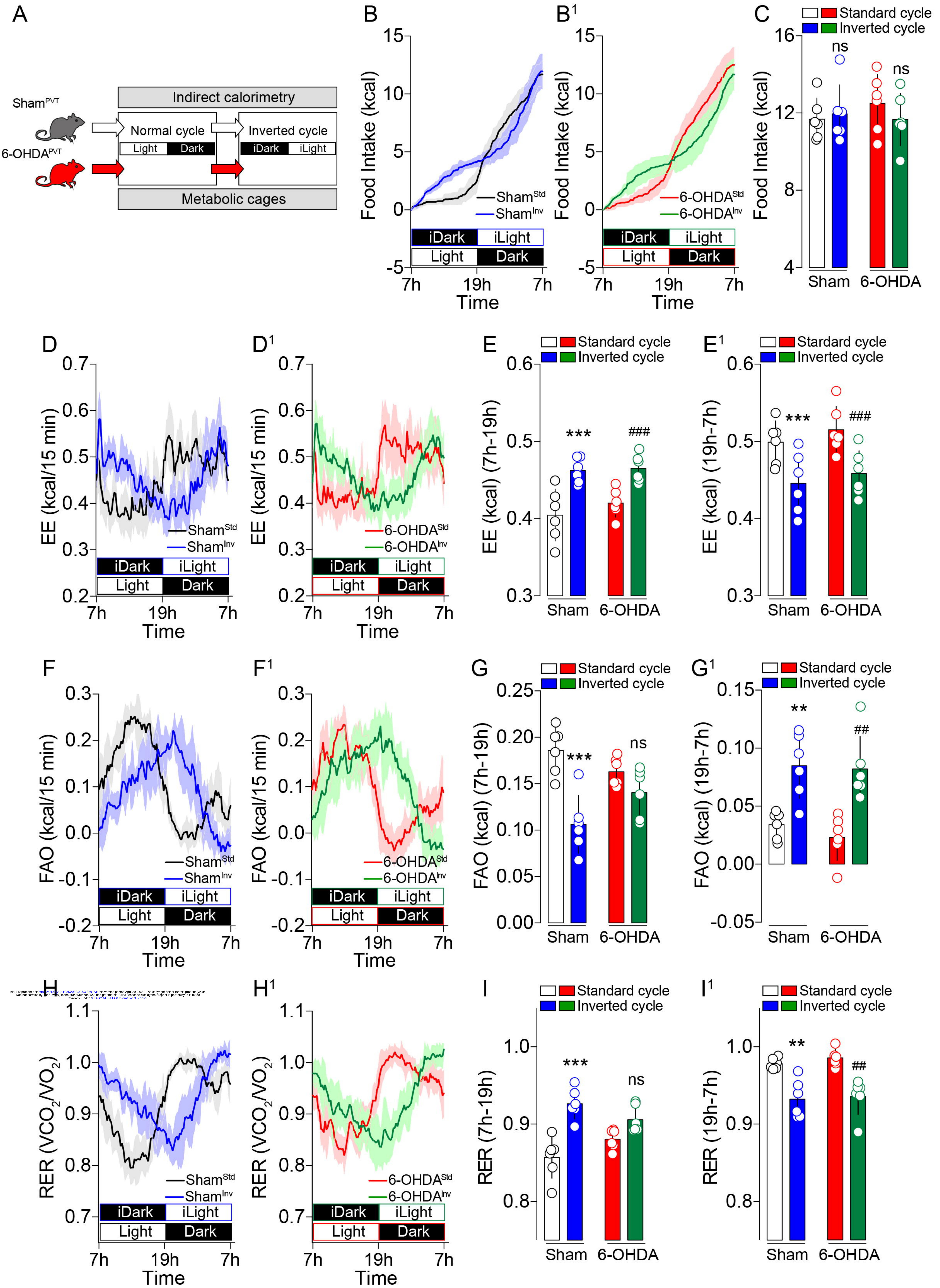


Figure 5

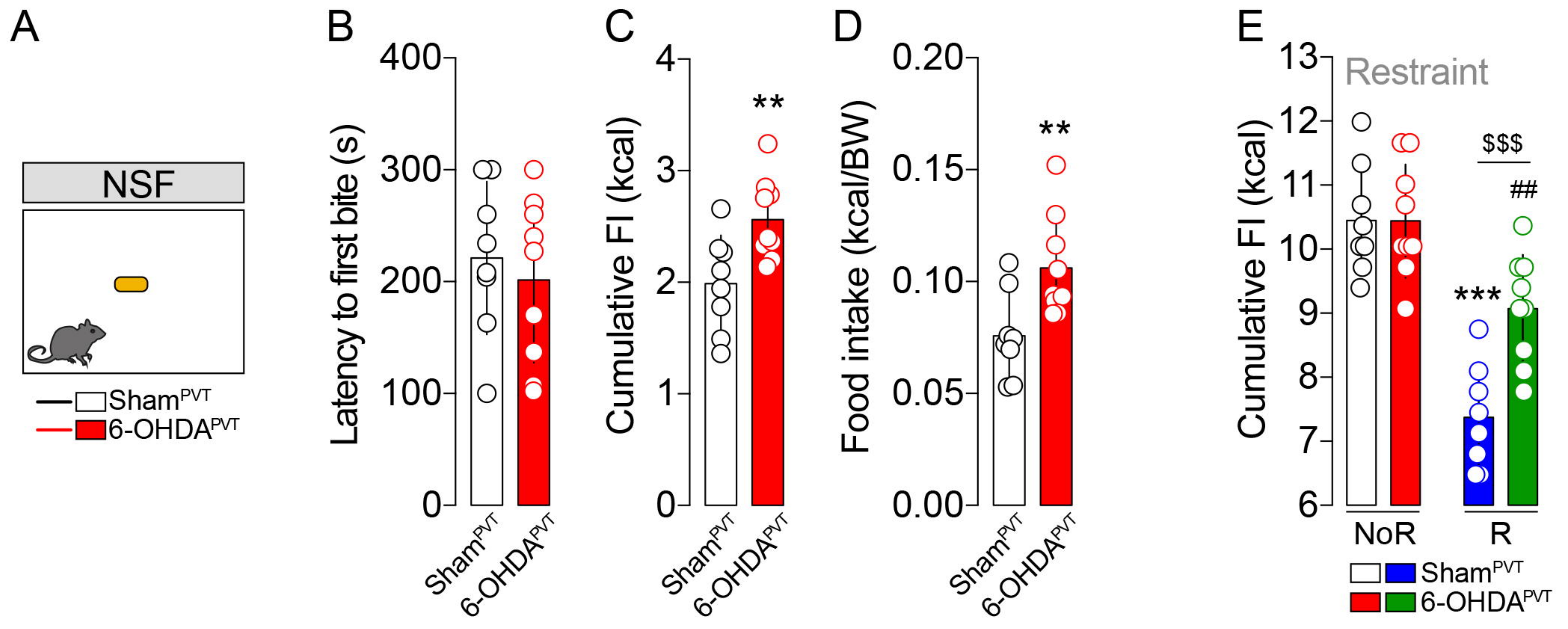


Figure 6

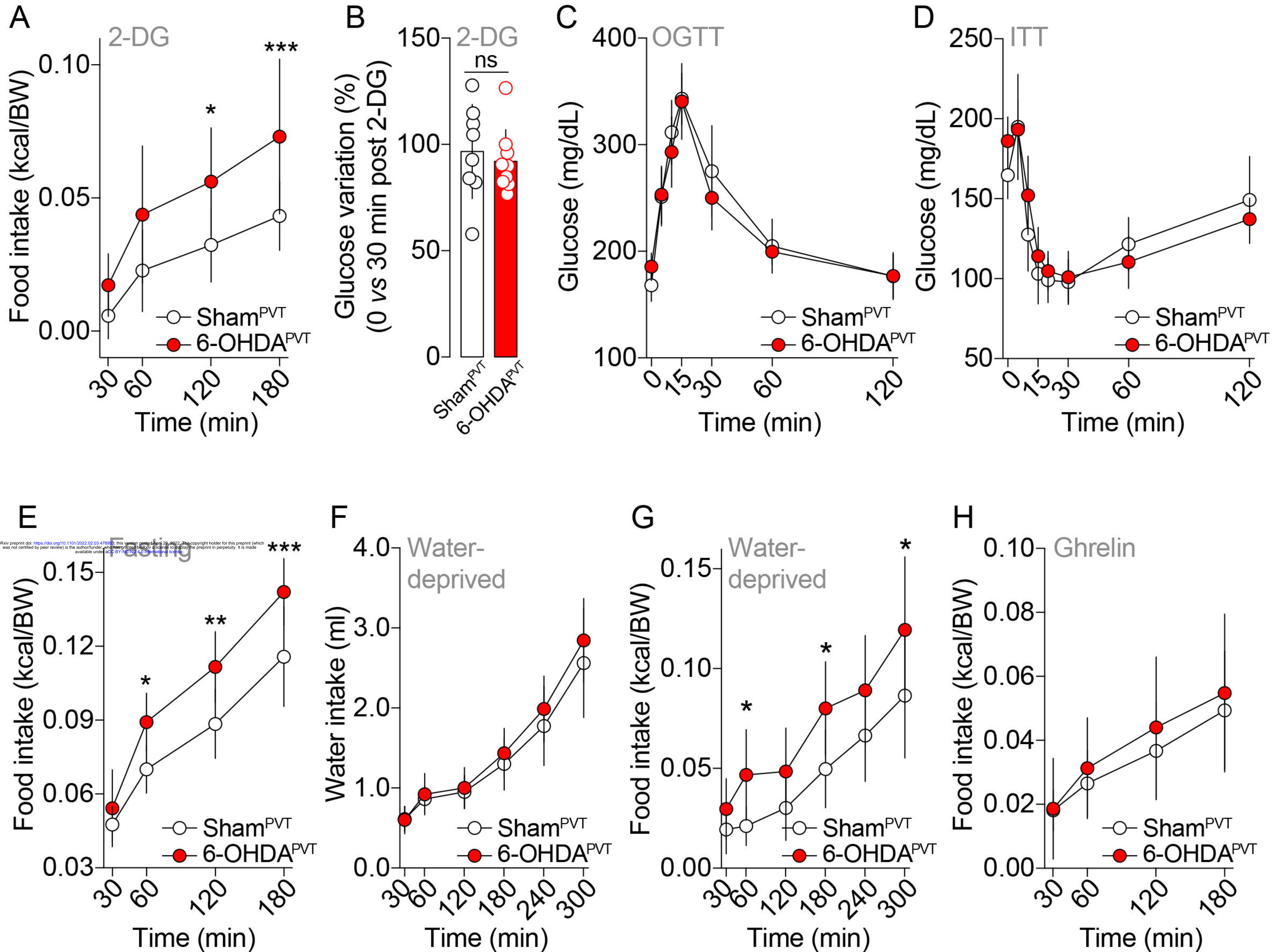
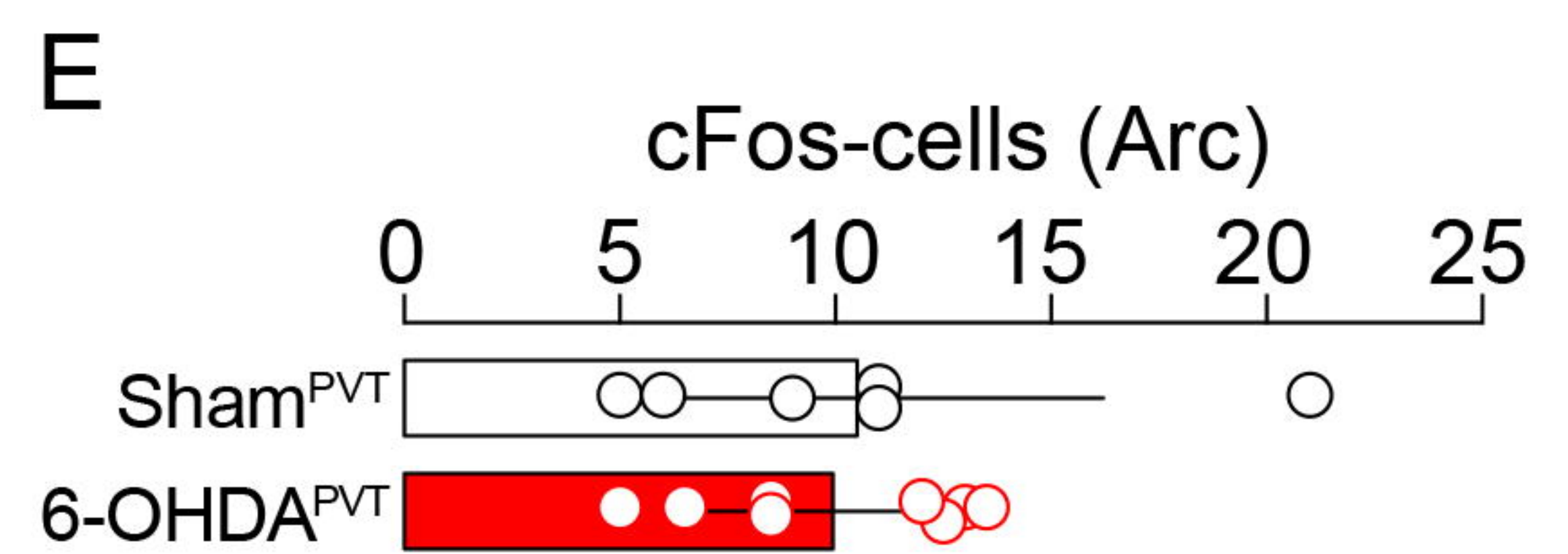
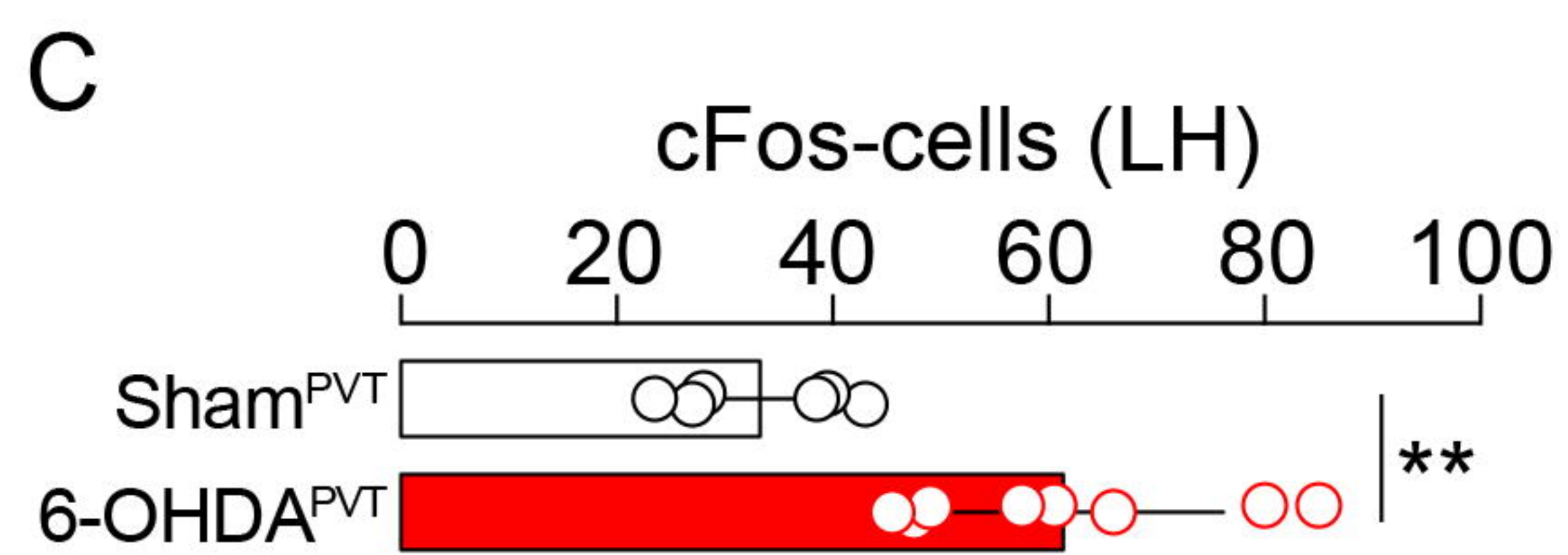
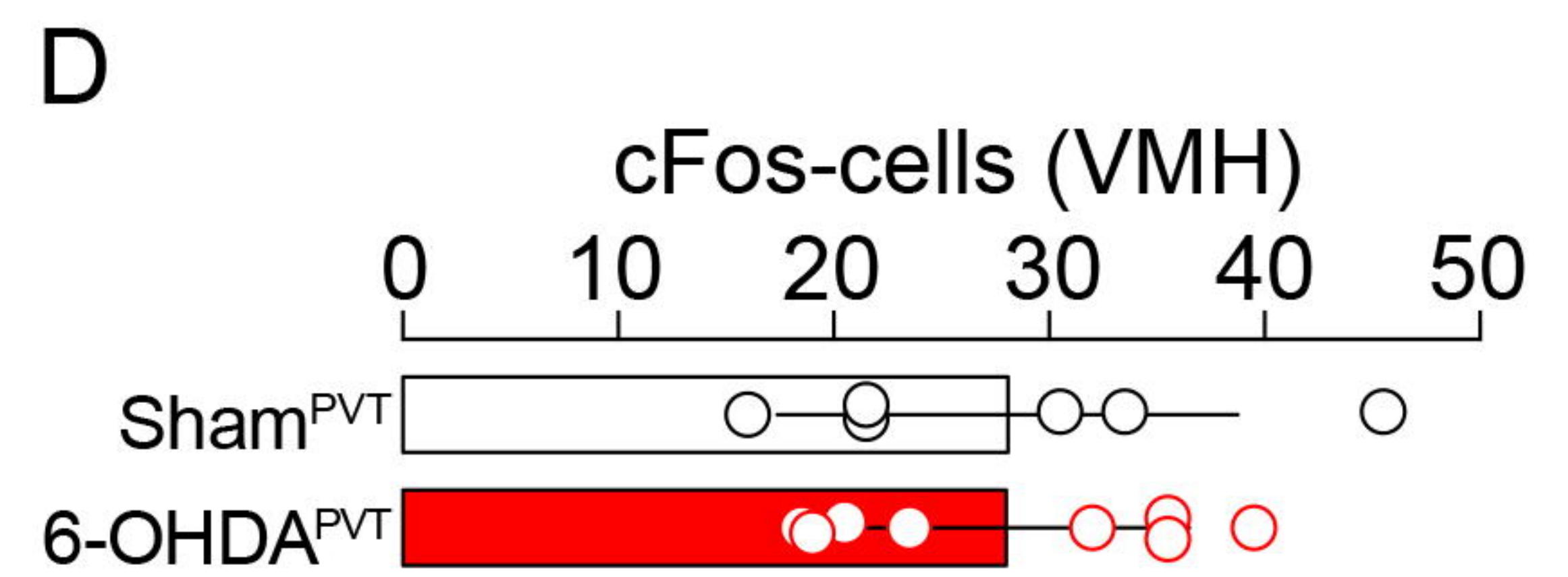
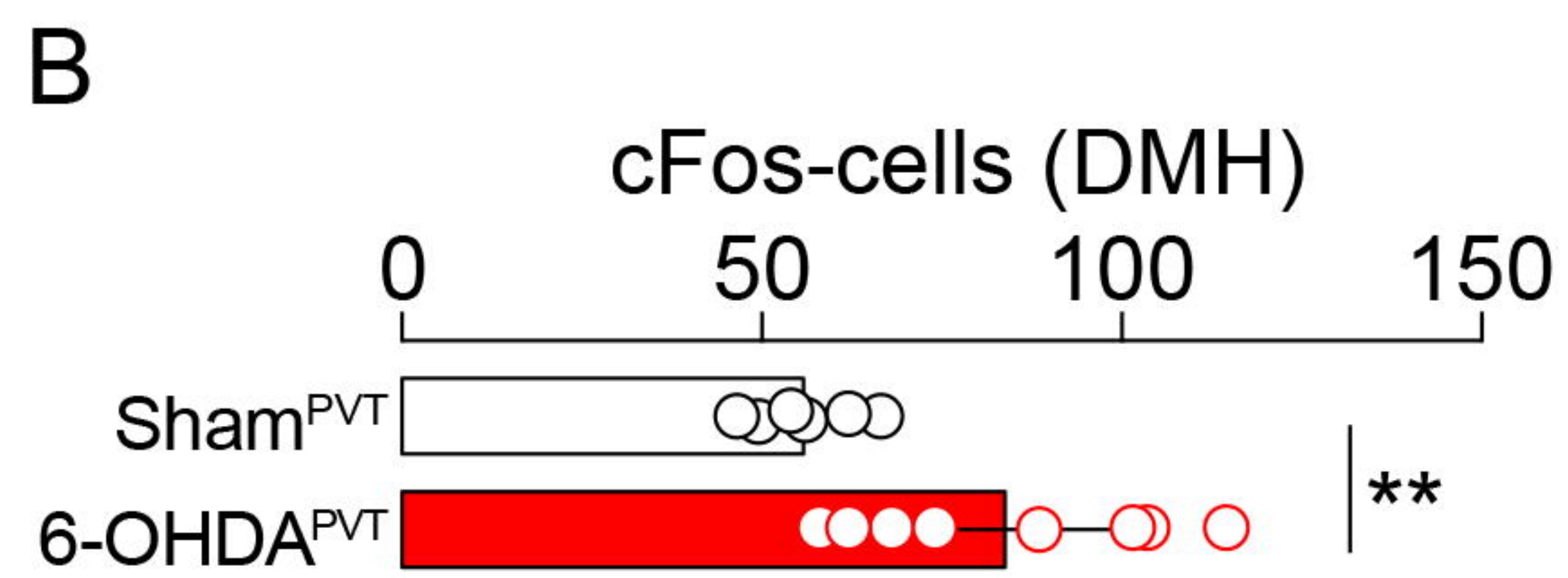
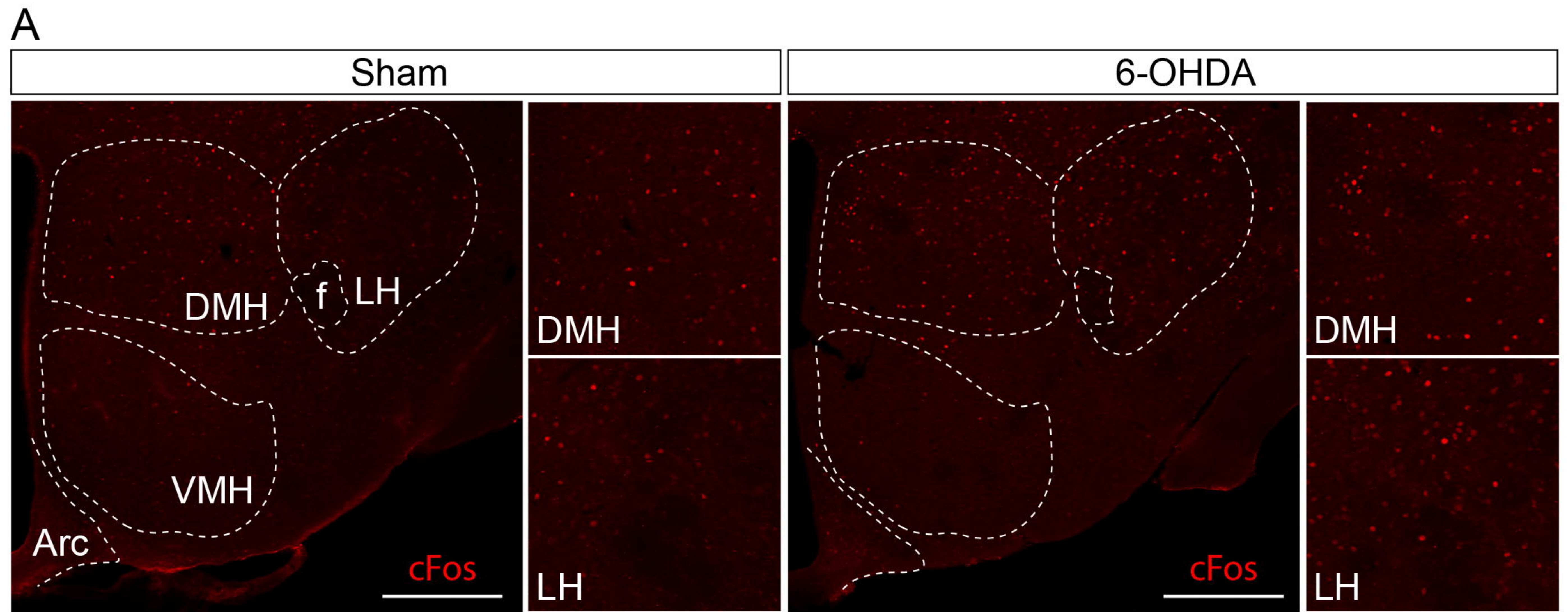


Figure 7



bioRxiv preprint doi: <https://doi.org/10.1101/2022.02.03.478953>; this version posted April 29, 2022. The copyright holder for this preprint (which was not certified by peer review) is the author/funder, who has granted bioRxiv a license to display the preprint in perpetuity. It is made available under aCC-BY-NC-ND 4.0 International license.

